PHOTOELASTIC STUDY OF INTERRUPTED PRESSURE VESSEL FRAMES

BY

JAMES CLEMENT BALLANTINE, JR.
LIEUTENANT COMMANDER, UNITED STATES NAVY
B.S., UNITED STATES NAVAL ACADEMY
(1957)

SUBMITTED IN PARTIAL FULFILLMENT OF THE REQUIREMENTS
FOR THE DEGREE OF NAVAL ENGINEER
AND THE DEGREE OF
MASTER OF SCIENCE IN NAVAL ARCHITECTURE
AND MARINE ENGINEERING

AT THE

MASSACHUSETTS INSTITUTE OF TECHNOLOGY

JUNE, 1967

PHOTOELASTIC STUDY OF INTERRUPTED PRESSURE VESSEL FRAMES

BY

JAMES CLEMENT BALLANTINE, JR.
LIEUTENANT COMMANDER, UNITED STATES NAVY
B.S., UNITED STATES NAVAL ACADEMY
(1957)

SUBMITTED IN PARTIAL FULFILLMENT OF THE REQUIREMENTS
FOR THE DEGREE OF NAVAL ENGINEER
AND THE DEGREE OF
MASTER OF SCIENCE IN NAVAL ARCHITECTURE
AND MARINE ENGINEERING

AT THE

MASSACHUSETTS INSTITUTE OF TECHNOLOGY

JUNE, 1967

PHOTOELASTIC STUDY OF INTERRUPTED PRESSURE VESSEL FRAMES

by

JAMES CLEMENT BALLANTINE, JR.
LIEUTENANT COMMANDER, UNITED STATES NAVY

Submitted to the Department of Naval Architecture and Marine Engineering on 19 May 1967 in partial fulfillment of the requirements for the Master of Science Degree in Marine Engineering and Naval Architecture and the Professional Degree, Naval Engineer.

ABSTRACT

The objective of this thesis is to obtain an understanding of the variation in stress on the cardinal axes of a circular penetration with elliptical reinforcements in a simulated stiffened cylindrical pressure vessel. The size and location of the circular penetration is such that the continuity of one of the ring frames has been destroyed.

The biaxial compressive loading of a pressure vessel has been obtained by superimposing the stress distribution obtained on the free boundary with a loading parallel to the ring frames representing hoop stress and the stress distribution obtained with a loading at right angle to the ring frames representing longitudinal stress.

By a systematic variation of the reinforcement geometry and the weight of reinforcement material, the relationship between the stress concentration factors, geometry, and weight of material has been investigated.

The photoelastic method of experimental stress analysis was chosen as the means of carrying out the investigation. The standard crossed circular polariscope was used in studying the isochromatic fringe patterns.

The two dimensional models were constructed with PS-5 material from Photolastic, Incorporated. All models were built upon a basic foundation of 4" x 4" x $\frac{1}{4}$" material with a central $1\frac{1}{4}$" diameter circular hole.

The effects of the various geometries and weights of reinforcement were investigated by using three basic families of geometrical shapes in which a sequence of five steps in the reinforcement thicknesses were made for each family.

For the particular series of geometries investigated, the best geometry for the reinforcement is the circular family which consisted of models 3, 6, 9, 12, and 15. This series shows the lowest stress concentration factors for a given thickness or weight of reinforcement material.

A comparison was made between the stress obtained by a strain gage and the stress obtained by photoelastic analysis. The result showed close agreement between the two techniques of experimental stress analysis.

The complicated interrelationships of all the variables that ultimately specify the geometries associated with a penetration in a stiffened cylindrical pressure vessel indicate that today each specific configuration must be analyzed on an individual basis.

To attempt to interrelate such parameters as pressure vessel thickness, frame size, frame shape, frame spacing and penetration size in order to obtain an all inclusive design procedure for optimum reinforcement would appear to require an extensive model testing program. These results might then serve as a basis from which to devise design procedures.

Thesis Supervisor: J. Harvey Evans

Title: Professor of Naval Architecture

ACKNOWLEDGEMENTS

The author is sincerely grateful for the guidance as thesis supervisor of Professor J. Harvey Evans, Department of Naval Architecture and Marine Engineering, and as advisor of Professor William M. Murray, Department of Mechanical Engineering.

The author would like to express his appreciation to Professor Evans for suggesting this area of investigation by use of the techniques of photoelasticity, and to Professor Murray for his advise on photoelastic materials and techniques and for permission to use the equipment of the Experimental Stress Analysis Laboratory.

TABLE OF CONTENTS

INDEX OF FIGURES

INDEX OF TABLES

LIST OF APPENDICES

NOMENCLATURE

A - A Photoelastic Constant of the Material

a - The Amplitude of Light Vibration

B - A Photoelastic Constant of the Material

C - The Differential Stress Optical Constant or
The Compression Region

D - Diameter

E - Modulus of Elasticity

f - Fringe Constant of the Photoelastic Material or
Frequency of Vibration

h - Thickness of the Photoelastic Material

n - Order of Interference

N_o - Refractive Index of Unstressed Material

N_1 - Refractive Index on Number One Principal Plane

N_2 - Refractive Index on Number Two Principal Plane

P - Proportionality Factor of $2\pi f$

PS-5 - Manufactures Designation of the Photoelastic Material

S - A Light Vector

SCF - Stress Concentration Factor

T - Tension Region

t - Time

t_1 - Time Required for Transmission on the No. 1 Principal Plane

t_2 - Time Required for Transmission on the No. 2 Principal Plane

V - Velocity of Transmission in the Surrounding Medium

V_1 - Velocity of Transmission on the No. 1 Principal Plane

V_2 - Velocity of Transmission on the No. 2 Principal Plane

α - Angle Between the Original Plane of Vibration and the No. 1 Principal Plane

δ_1 - Change of Refractive Index on the No. 1 Principal Plane

δ_2 - Change of Refractive Index on the No. 2 Principal Plane

σ_1 - The Algebraically Larger Principal Stress

σ_2 - The Algebraically Smaller Principal Stress

σ_t - The Tangential Principal Stress Along a Free Boundary

σ_n - The Normal Principal Stress Along a Free Boundary

$\mu\varepsilon$ - Microstrain

I. INTRODUCTION

The presence of a circular hole in a flat plate loaded in its own plane results in an increase of the stress concentration. If the hole is small compared with the lateral dimensions of the plate its effect on the stress distribution will be nearly local. A finite plate with lateral dimensions several times greater than the hole diameter is of adequate size. The effect of a suitable reinforcement of the hole is to decrease this stress concentration so that when the stress in the plate is nowhere to exceed a given value the presence of the reinforcement results in a decrease in the necessary weight of the structure. The design of a reinforcement is therefore an important problem when the weight of the structure must be as low as possible, as, for example, holes in pressure hulls of submarines.

The object of this thesis is to obtain an understanding of the stress variation around a circular penetration with elliptical reinforcements in a framing system subjected to a loading that is representative of that present in a pressure vessel. A pressure vessel was simulated by loading the model in line with the framing system to represent hoop stress, and then turning the model ninety degrees and applying half the loading so as to represent longitudinal stress.

The ratio of the superimposed stresses on the vertical and horizontal axes of the free inner circular boundary is considered to be a stress concentration factor that indicates the efficiency with which the reinforcement material has been utilized. Ideally all the components of a structure work at

similar stress levels so there is no wasted material capabilities.

In recent years the advancing technology in several areas has required hardware in which large penetrations have been needed in a stiffened cylindrical pressure vessel. Most of these applications have been in systems that are weight limited with regard to the amount of material that can be placed in the structure itself, thereby detracting from the desired payload of the vehicle. Even with the advent of high strength-to-weight ratio structural materials, the need for optimizing the geometry of reinforcement is important so that the material is utilized in the most efficient manner.

The photoelastic stress analysis technique was chosen for this investigation since it provides a means of determining the stresses in two-dimensional problems that cannot be solved analytically. The results obtainable have an accuracy in irregular members that is comparable to the results obtained with precise strain gage techniques. In the process of developing a satisfactory design, photoelastic analysis provides a means of readily obtaining qualitative results for the locations of minimum and maximum stresses and for the determination of changes in stress distribution caused by minor alterations in the shape of the model.

To permit the use of two-dimensional photoelasticity, the assumption that the radius of the pressure vessel is relatively large with respect to the frame spacing has been made. Small radii cylinders would probably require the use

of three-dimensional photoelastic analysis. This technique requires the freezing of the stresses in the model and then subsequently cutting the model apart in order to view the stress patterns.

This thesis is an effort to show, through two-dimensional photoelastic analysis, the effect of reinforcements in a biaxial loading condition.

In order to investigate the effect of reinforcements that formed part of a simulated stiffened cylinder, three families of geometrical shapes for the reinforcements were used. These reinforcements were added to three basic models. Each of these three basic models were identical with regard to intact ring frames and the circular hole. Each model was built up from a four inch by four inch square foundation piece that was one quarter inch thick and had a one and one quarter inch diameter hole in the center. Each model to which the reinforcements were to be added had two strips to represent ring frames cemented to each side near opposite edges of the models.

The geometrical variation in the reinforcements to be cemented in way of the central hole all had an inside diameter of one and one quarter inches to match the foundation piece hole. The systematic variation of the outer edge of the reinforcements consisted of three ratios for the major to minor axes of an ellipse. The ratios used were one to one (a circle), one and one quarter to one, and one and one half to one. All these reinforcements were 0.080 inches thick. They were cemented to their respective foundation

piece and analyzed in five steps which consisted of 2, 3, 4, 5 and 6 thicknesses. For further description of the models see Appendix B.

II. PROCEDURE

The primary objective of this thesis is to investigate the stress distributions around a circular penetration that is of sufficient size that it has resulted in a discontinuity in a ring frame of a stiffened cylindrical pressure vessel. The photoelastic models which contain this penetration include the two immediately adjacent simulated ring frames. The specific stresses of interest on this interior free boundary are those on the horizontal and vertical axes. The vertical axis is the axis parallel to the framing system. The specific values used in determining the ratio of the stresses on these two axes are the average of the two values on each individual axis.

It was not necessary to determine the stress levels within the model as the region of interest was the interior free boundary which will be the highest stressed material. The need to determine the isoclinic pattern of the model was therefore unnecessary. On any free boundary, the principal stress perpendicular to the boundary is zero, so only the tangential principal stress is present. The isochromatics on the edge represent the principal stress rather than the difference in principal stresses.

The isochromatic pattern was observed in a standard crossed circular polariscope using polarized light with a dark field. A more detailed discussion of procedure and photoelastic techniques is found in Appendix A and B.

The models were machined from Photolastic Inc. PS-5 material using the high speed cutter in the Ship's

Structures Laboratory. Aluminum templates to guide this cutter were made using larger plywood templates on a pantograph. A more detailed discussion of the steps in the preparation and construction of the models is contained in Appendix B.

Each model was placed in the loading frame described in Appendix B in which uniform compression was applied to the model on the upper and lower edges. The force applied to the model in line with the ring frames was twice the force applied on the other two edges when the model was turned ninety degrees.

This two to one force balance was a simulation of the relationship of hoop stress to longitudinal stress in an unstiffened pressure vessel. The loads for model number one were 1,000 pounds and 500 pounds. For the other models this ratio of two to one was obtained using 700 pounds for the hoop loading and 350 pounds for the longitudinal loading. There was somewhat of a trade off in the loading values. Too high a loading in line with the frames makes the estimation of fractional fringe orders extremely difficult while too low a loading in line with the frames would give only a few fringe orders when this value is halved for the loading perpendicular to the frames. Buckling was not a problem with the models since the sensitivity of PS-5 results in adequate fringes at a moderate load.

The need to estimate the fringe orders to the nearest one-quarter order led to the use of Polaroid Type 55 P/N

film which gives both a positive and a negative. The negative was projected on a screen with an overhead projector so as to magnify the fringe pattern as an aid to accurate determination of the fractional fringe orders on the circular hole axes. The values of the fringes on the axes and the respective stress levels are given in Tables VIII to XI and XVII to XX of Appendix C. The photographic records of the fringe patterns are in Appendix D in Figures XVII to XXII.

To determine the fringe constant for the material, two disk compression specimens were machined. The fringe constant is a function of the material and the wavelength of the monochromatic light source. Mercury green light was used in this experiment.

A more detailed discussion of the determination of the fringe constant is given in Appendix B.

III. GRAPHICAL PRESENTATION

OF RESULTS

FIGURE X

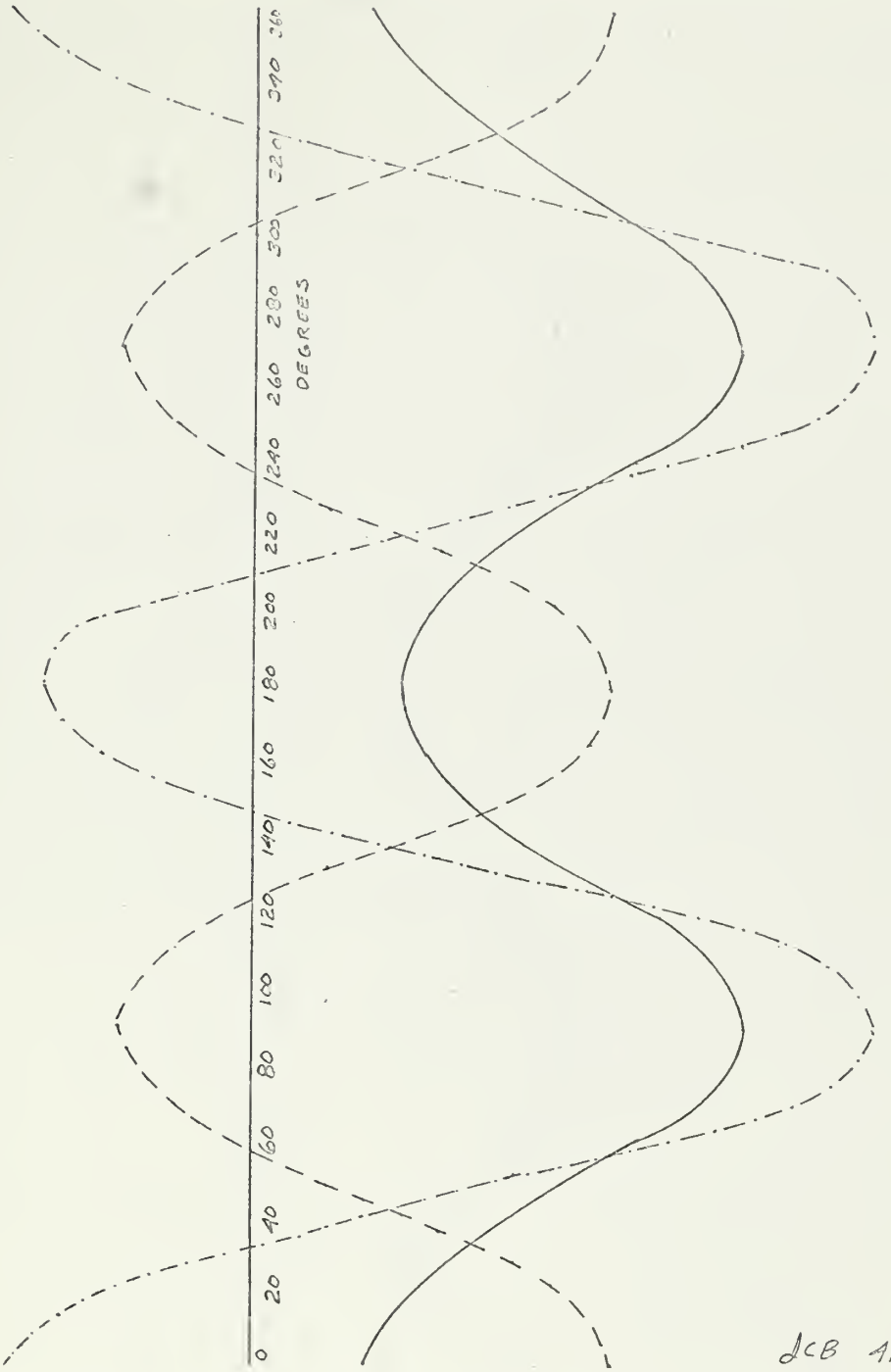

JCB 4/15/67

8 6 4 2 0 2 4 6 8 10 12 14 16 18

TENSION - FRINGE ORDER - COMPRESSION

-·-·- 1000 LB HOOP LOADING
- - - - - 500 LB LONGITUDINAL LOADING
——— SUPERPOSITION OF BOTH

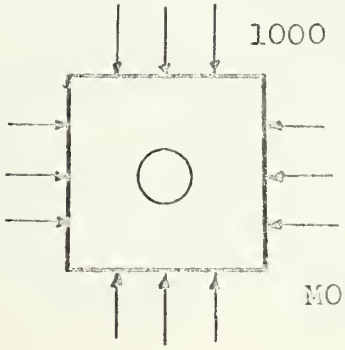

MODEL NO. 1

BOUNDARY STRESSES IN FRINGES
VS
ANGULAR POSITION IN DEGREES
FOR INSIDE CIRCULAR BOUNDARY

FIGURE IX

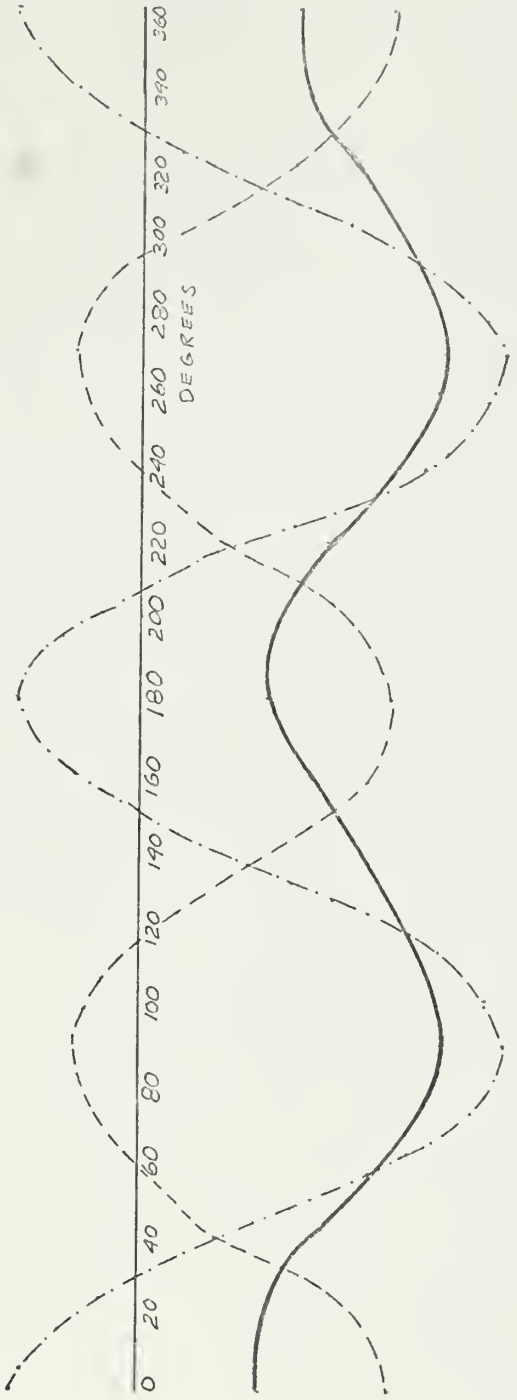

JCB 4/15/67

8 6 4 2 0 2 4 6 8 10 12 14 16 18

TENSION - FRINGE ORDER - COMPRESSION

-·-·-·- 700 LB HOOP LOADING
- - - - - - 350 LB LONGITUDINAL LOADING
——— SUPERPOSITION OF BOTH LOADINGS

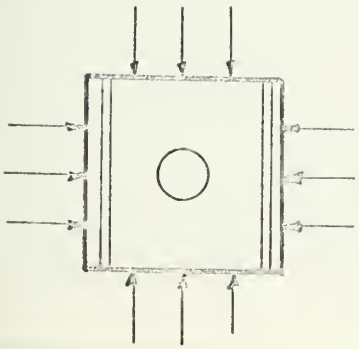

700 LBS

350 LBS

BOUNDARY STRESSES IN FRINGES
VS
ANGULAR POSITION IN DEGREES
FOR INSIDE CIRCULAR BOUNDARY

MODEL NO. 2

FIGURE III

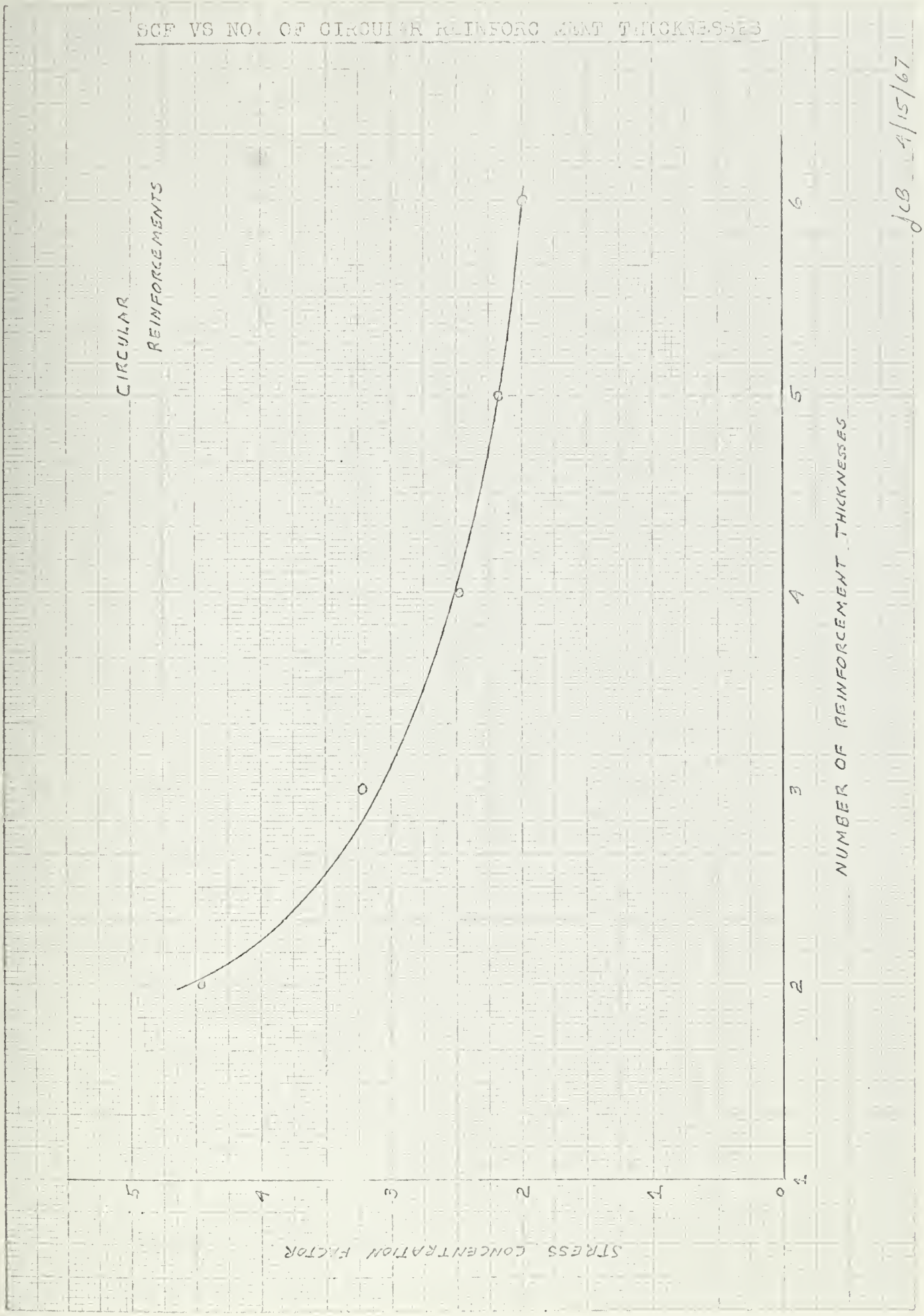
SCF VS NO. OF CIRCULAR REINFORCEMENT THICKNESSES
CIRCULAR REINFORCEMENTS
JCB 4/15/67
NUMBER OF REINFORCEMENT THICKNESSES
0
1
2
3
4
5
6
STRESS CONCENTRATION FACTOR
5
4
3
2
1
0

FIGURE IV

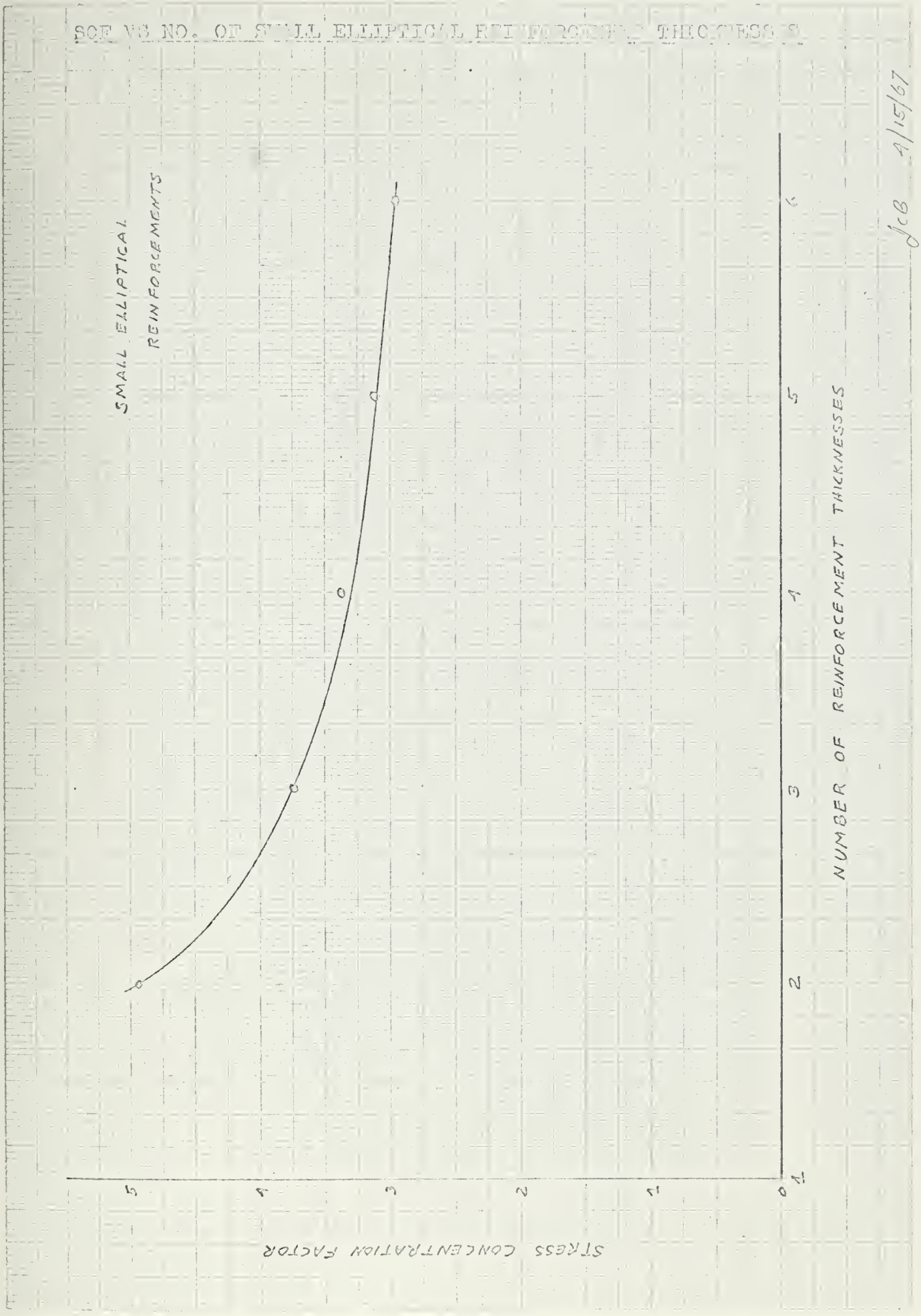
SCF VS NO. OF SMALL ELLIPTICAL REINFORCEMENT THICKNESS S
SMALL ELLIPTICAL
REINFORCEMENTS
NUMBER OF REINFORCEMENT THICKNESSES
STRESS CONCENTRATION FACTOR
0
1
2
3
4
5
JCB 4/15/67

FIGURE V

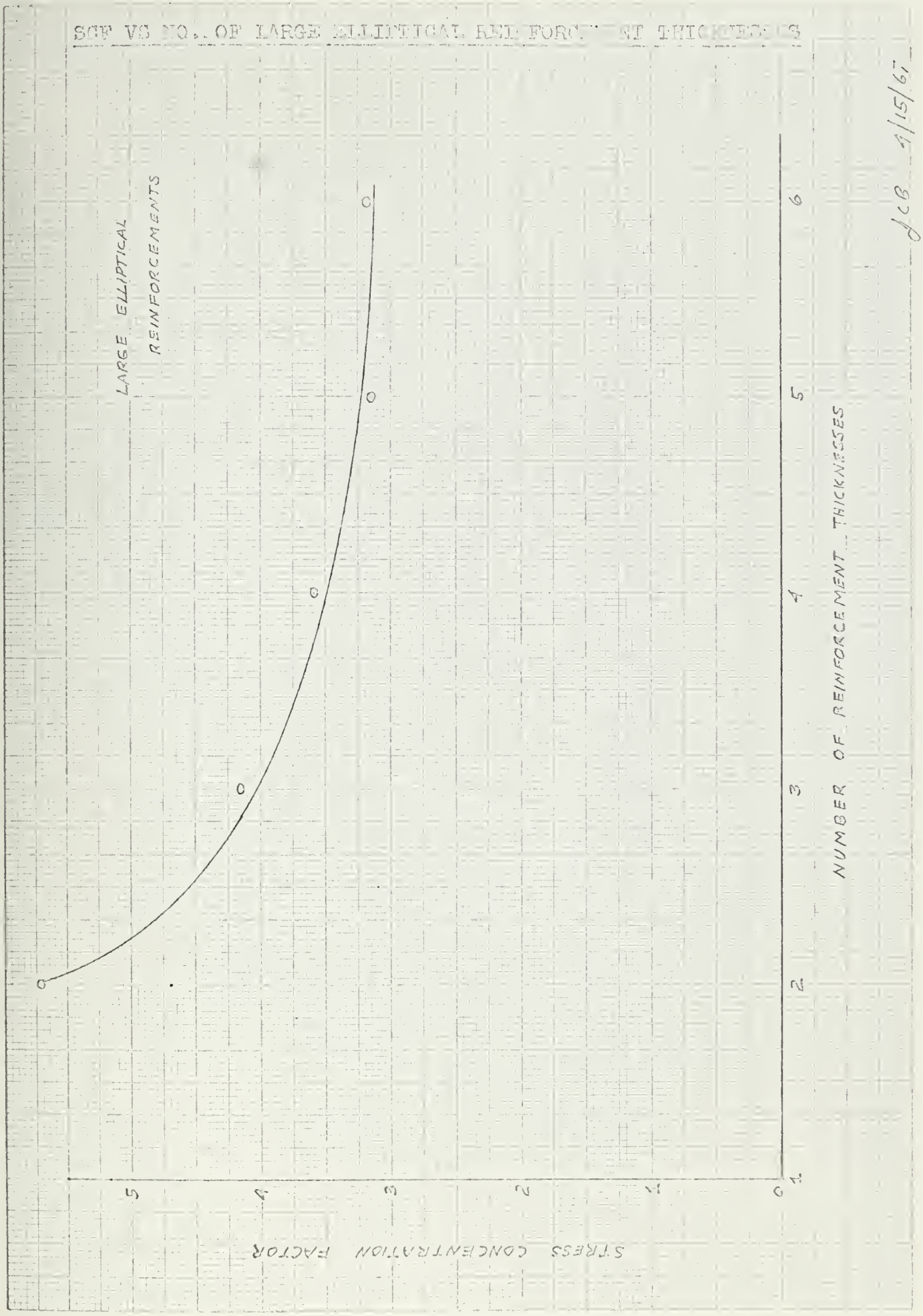
SCF VS NO. OF LARGE ELLIPTICAL REINFORCEMENT THICKNESS
LARGE ELLIPTICAL REINFORCEMENTS
STRESS CONCENTRATION FACTOR
NUMBER OF REINFORCEMENT THICKNESSES
0
1
2
3
4
5
6
JCB 4/15/67

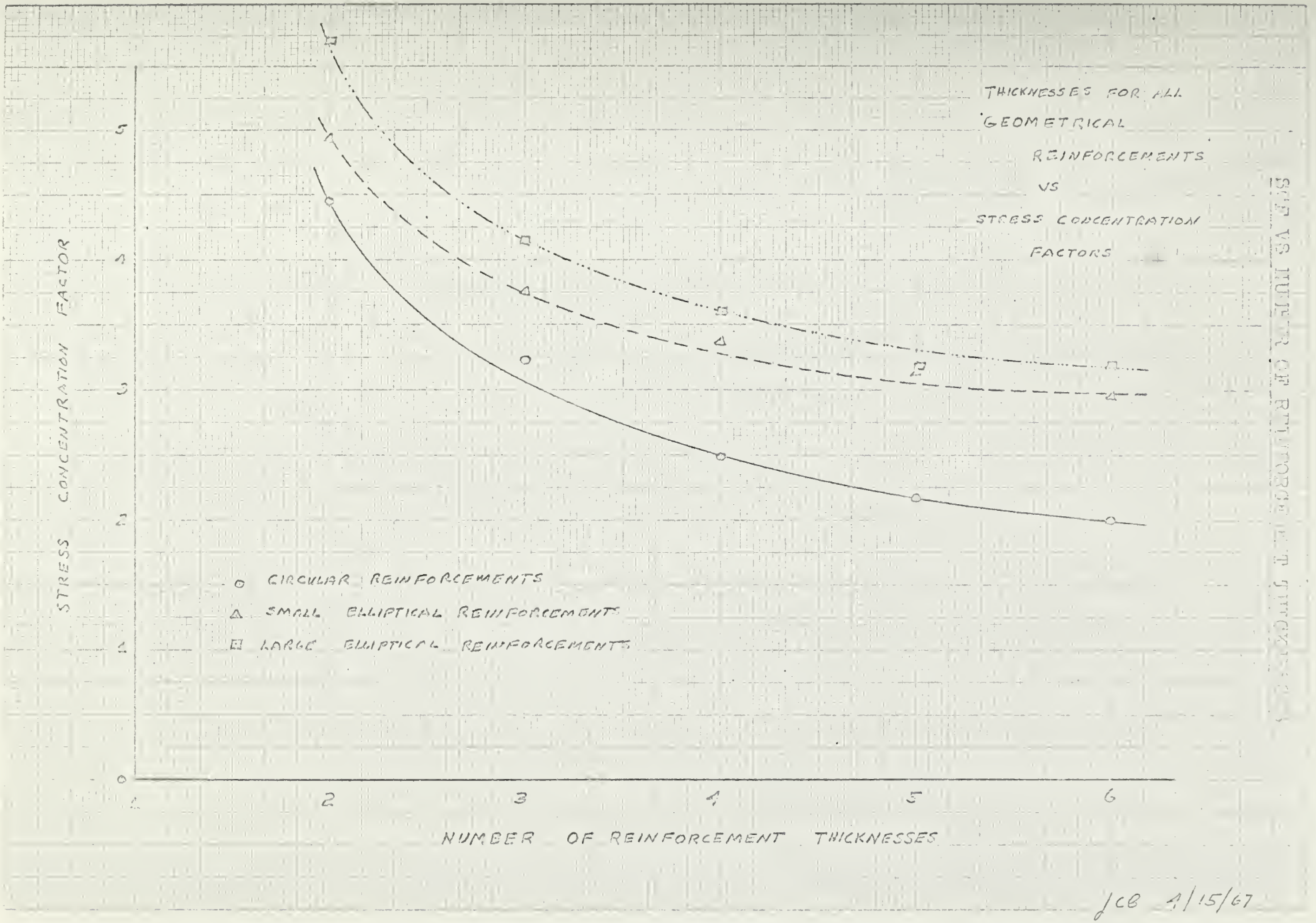

FIGURE VI

JCB 4/15/67

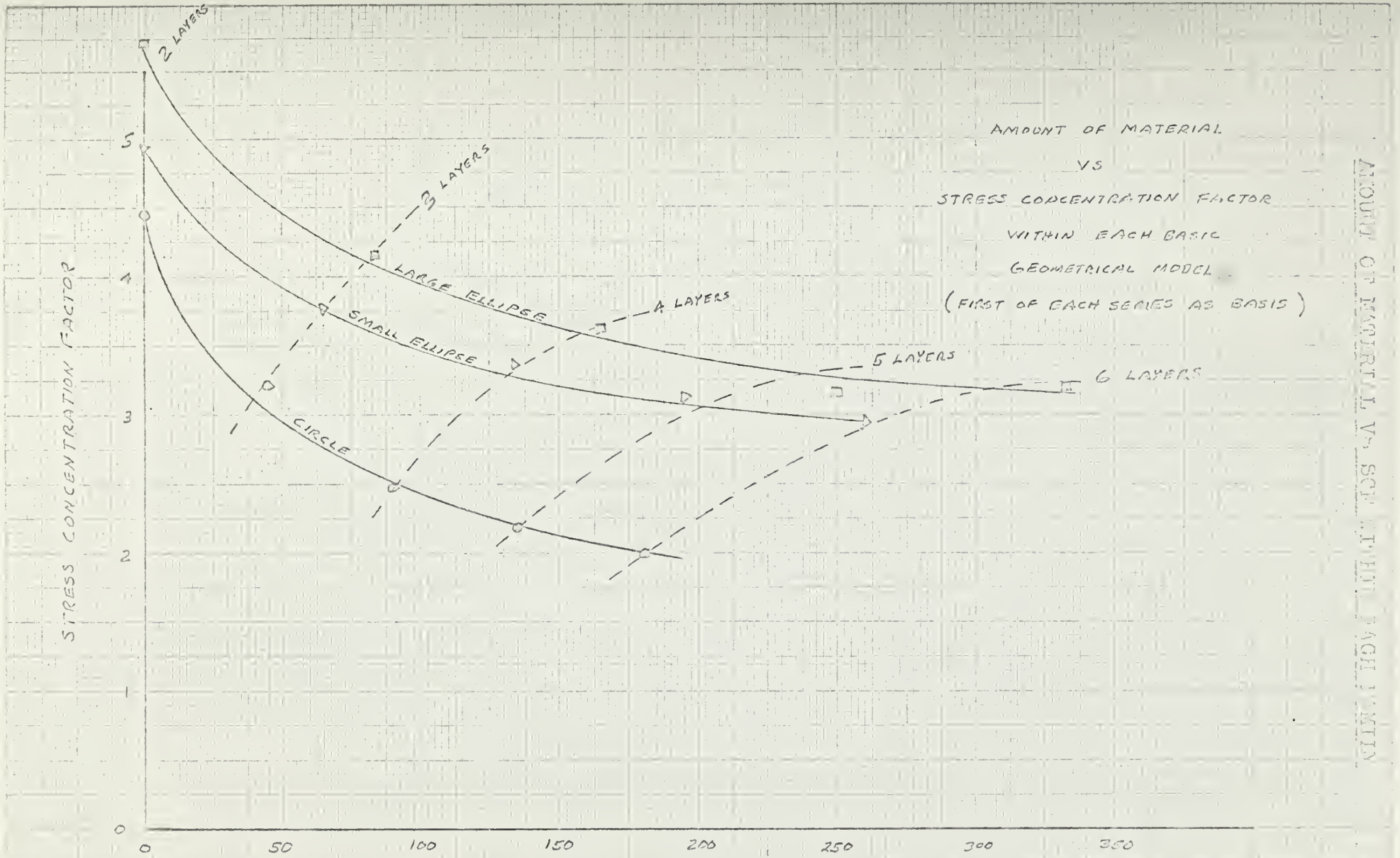

AMOUNT OF MATERIAL VS. SCF. WITHIN EACH BASIC

FIGURE VII

d'G 4/15/67

FIGURE VIII

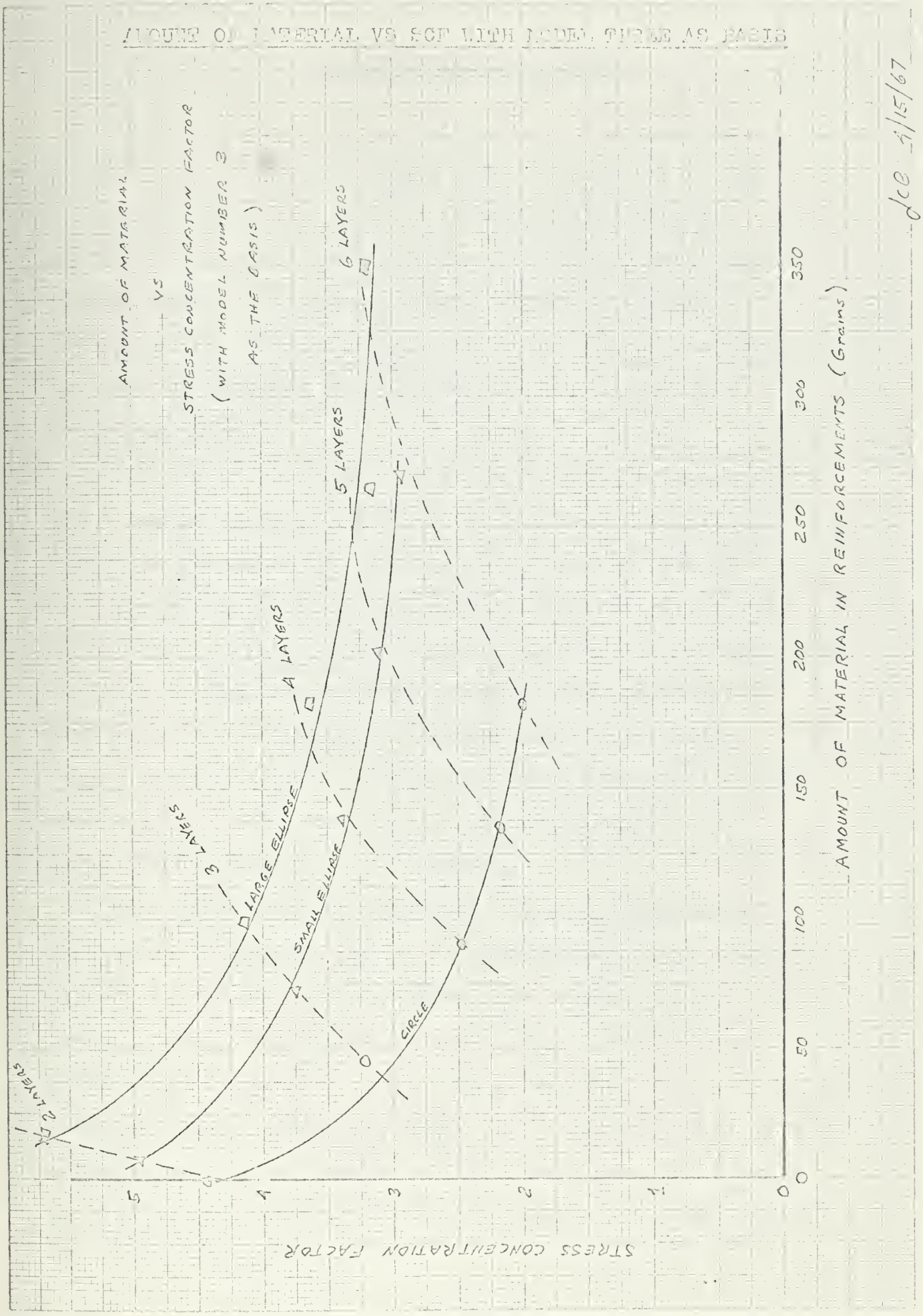
AMOUNT OF MATERIAL VS SCF WITH MODEL THREE AS BASIS
AMOUNT OF MATERIAL VS STRESS CONCENTRATION FACTOR (WITH MODEL NUMBER 3 AS THE BASIS)
6 LAYERS
5 LAYERS
4 LAYERS
3 LAYERS
2 LAYERS
LARGE ELLIPSE
SMALL ELLIPSE
CIRCLE
AMOUNT OF MATERIAL IN REINFORCEMENTS (Grams)
STRESS CONCENTRATION FACTOR
0
50
100
150
200
250
300
350
5
4
3
2
1
0
dco 4/15/67

IV. DISCUSSION OF RESULTS

In an experimental investigation of any sort, the accuracy of the results depend upon the accuracy of the raw experimental data and its interpretation through analysis. The end result of the analysis of these photo-elastic models is a stress concentration factor which represents the degree to which the reinforcement material has been distributed so as to be utilized in the most efficient manner.

The use of polaroid film which produces both a positive and a negative has aided the determination of the fringe orders at the points of interest. A magnification of over ten was obtained by projecting the negatives onto a screen for analysis. This magnification effect was necessary in order to resolve the small changes that resulted from each additional thickness of reinforcement on a basic family of models (ie. the circular reinforced family, etc.) and among the three families of models with the same number of reinforcement thicknesses.

The negatives became progressively more difficult to analyze as successive layers of reinforcement were cemented to each of the three basic geometrical shapes. There were several likely contributing factors that increased the difficulty of analysis. Any slight deviation from perfectly parallel light through the model due to imperfections in the grinding of the lens system of the polariscope would cause distortion of the fringes. As the thickness of the model

increased with successive reinforcement thicknesses the distortion became progressively worse. The glue layers and some small entrapped air bubbles tended to reduce the light transmission and thereby degrade the contrast of the photographs. Finally the slight misalignment of successive reinforcement rings tended to obscure the boundary fringe pattern.

By enlarging the negatives and taking into consideration the rate of change in fringe spacing as the free boundary was approached, the determination of the fringe order on the four cardinal axes was estimated to the nearest one quarter order. The higher the order at the point in question the more difficult the analysis of fractional fringe orders. One quarter order corresponds to an accuracy of $\pm$ 5% for five fringe orders or $\pm$ 2.5% for ten fringe orders. This accuracy is further impaired by the analysis problems mentioned above. The overall accuracy in the stress concentration factors is felt to be within $\pm$ 10% when considering all possible detrimental effects in the experiment.

The experimental results for models one and two have been plotted to show fringe order versus angular position around the entire free boundary of the circular hole. These plots in Figure I and II show the hoop and longitudinal loadings individually and then the superposition of the two. As expected the stress is compressive around the free boundary in the simulated pressure vessel.

The stress concentration factor for model one was at 3.72. The addition of the four strips of material that

represent the ring frames in model two reduced this stress concentration factor by a significant amount to 2.38. This indicates a considerable assumption of the load by the ring frames through shifting the load away from the circular hole when hoop loaded.

The results of the main sequence of experimental investigations are plotted in Figures III through VIII.. These figures are for the fifteen different models which made up the three families of basic geometrical shapes in which a sequence of five steps in the reinforcement thicknesses were made for each family. The stress concentration factors versus number of reinforcement thicknesses for each of the three basic families of reinforcement shapes are plotted individually in Figures III through V, and the three combined in Figure VI..

These figures show that of the reinforcement shapes investigated, circular reinforcment provides the smallest stress concentration factor for any given thickness.

The stress concentration factors versus amount(grains) of material in the reinforcements are shown in Figures VII and VIII. Figure VII is with the first of the five steps in each family as the reference points, while Figure VIII has model number three, which was the lightest reinforcement, as the reference point.

Clearly the circular reinforcements provide the least weight and lowest stress concentration factors for this particular overall geometry of a heavy ring frame stiffened cylindrical pressure vessel.

The trend in the ratio of major to minor axis in the elliptical shapes indicates that to further approach a stress concentration factor of one would require elliptical shapes in which the major axis is parallel to the longitudinal loading. The closer the stress concentration factor is to one, the more uniformily the material is being utilized in reinforcing the penetration.

The framing system of the pressure vessel will affect the specific geometry of the reinforcement that will prove to be optimum. Each particular frame size, frame spacing, and penetration will be a specific situation and require individual experimental stress investigations to optimize the usage of reinforcement material.

Upon completion of the use of the models, a cut was taken to true up the inside of the small elliptically reinforced model to permit mounting a strain gage on one side of the horizontal axis. The model was then loaded in line with the frames and the stress level determined by both the photoelastic technique and the strain gage. Surprisingly, those values gave stress levels that differed by only about 1%. This result showed a remarkable degree of agreement in the two techniques of experimental stress analysis.

V. CONCLUSIONS

For the particular series of geometries investigated, the best type of reinforcement is the circular family which consisted of models 3, 6, 9, 12 and 15. This series shows the lowest stress concentration factors for a given thickness or weight of reinforcement material. The lower the stress concentration factor, the more uniformly the reinforcement material is being utilized.

The problem investigated here has been the reinforcement of a circular hole in such a way that it is as nearly as possible equivalent to the structure without the hole. A perfect equivalence would mean that the stresses and displacements of the structure would remain the same as those which would have appeared without the hole.

The trend in the relationship between geometrical shape and the stress concentration factor indicates that the likely orientation for a stress concentration factor closer to one would be obtained with an ellipse having the major axis perpendicular to the ring frames for this heavily stiffened cylindrical pressure vessel. As heavy ring frames tend to carry more of the hoop loading, it becomes necessary to provide additional reinforcement material to carry part of the longitudinal loading if it is desired to have uniform peak stresses on the cardinal axes.

A comparison of the photoelastic and strain gage techniques of experimental stress analysis has shown very close agreement between the two methods.

VI. RECOMMENDATIONS

The results of this investigation indicate that further photoelastic analysis in this general area may be beneficial. Since the complicated geometrical nature of stiffened cylinder frame and reinforcement interactions apparently preclude theoretical analysis, a recommended area of study that might will have preceded this investigation would be to investigate a sequence of geometrical reinforcements in a simulated pressure vessel loading without ring frames. The superposition technique for representing the biaxial loading would be used. These results would then be uncluttered by ring frame sizes and spacing and might very well serve as a beginning step in ultimately devising design procedures relating all parameters.

The complicated interrelationships of all the variables that ultimately specify the geometries associated with a penetration in a stiffened cylindrical pressure vessel indicate that today each specific configuration must be analyzed on an individual basis.

To attempt to interrelate such parameters as pressure vessel thickness, frame size, frame shape, frame spacing and penetration size in order to obtain an all inclusive design procedure for optimum reinforcement would appear to require an extensive model testing program. These results might then serve as a basis from which to devise design procedures.

VII. APPENDIX

A. SUPPLEMENTARY INTRODUCTION

1. Fundamentals of Photoelasticity

Many transparent materials such as glass, bakelite, and most other synthetic resins display the same double-refracting optical effect on a beam of light as a crystal when these materials are subjected to stress. Examination of these stressed materials under polarized light reveals colored patterns which are caused by the optical retardation of the light passing through the material. The retardation depends on the nature and intensity of the stress. Upon removal of the load, the double refraction disappears. The stress optical calibration factor (fringe constant) is obtained for the specific material from a geometrical shape and loading for which the theoretical stress distribution is known.

For normal incident light on a flat plate subjected to plane stress within the elastic limit, the light transmission follows two principles which form the basis for photoelastic stress analysis. These two principles are:

(1) When light is transmitted through a stressed photoelastic material, it is polarized into two components at right angles to each other and is transmitted only on the planes of principal stress.

(2) The velocity of transmission in each principal plane of stress is dependent on the magnitudes of the principal stresses in these two planes.

For the case of light which is traveling in the normal direction to the plane of a sheet of photoelastic material

which is subjected to a condition of plane stress, we have the following quantitative relationship between the stress and the optical effect in terms of the change of index of refraction caused by the presence of the stress:

$$\delta_1 = N_1 - N_0 = A\sigma_1 + B\sigma_2 \qquad (1)$$

$$\delta_2 = N_2 - N_0 = B\sigma_1 + A\sigma_2 \qquad (2)$$

where:

δ_1 - Change of Refractive Index on No. 1 Principal Plane

δ_2 - Change of Refractive Index on No. 2 Principal Plane

N_0 - Refractive Index of Unstressed Material

N_1 - Refractive Index on No. 1 Principal Plane

N_2 - Refractive Index on No. 2 Principal Plane

σ_1 - The Algebraically Larger Principal Stress

σ_2 - The Algebraically Smaller Principal Stress

A & B - Photoelastic Constants of the Material

By subtracting equation (2) from equation (1), one finds that the difference between the refractive indices on the two principal planes is:

$$\delta_1 - \delta_2 = N_1 - N_2 = (A - B)(\sigma_1 - \sigma_2)$$

$$N_1 - N_2 = C(\sigma_1 - \sigma_2) \qquad (3)$$

where:

C - The Differential Stress Optical Constant

When light passes from one medium into another of different density, a change in velocity results. The ratio of these two velocities is called the index of refraction. By dividing the velocity of light in the first medium by the velocity of light in the second medium we obtain the two relationships:

$$N_1 = V/V_1 \quad \text{and} \quad N_2 = V/V_2 \qquad (4a,b)$$

where:

V - Velocity of Transmission in the Surrounding Medium

V_1 - Velocity of Transmission on the No. 1 Principal Plane of Stress

V_2 - Velocity of Transmission on the No. 2 Principal Plane of Stress

By substituting equation (4) into equation (3) we have:

$$N_1 - N_2 = \frac{V}{V_1} - \frac{V}{V_2} = \frac{V(V_2 - V_1)}{V_1 V_2} = C(\sigma_1 - \sigma_2)$$

Therefore:

$$\sigma_1 - \sigma_2 = \frac{V}{C}\left(\frac{V_2 - V_1}{V_1 V_2}\right) \qquad (5)$$

Thus the differences in the velocities of transmission in the planes of the principal stresses is seen to be directly proportional to the difference of the two principal stresses $(\sigma_1 - \sigma_2)$.

2. The Polariscope and the Photoelastic Effect

The optical system most frequently used to produce the necessary polarized beams of light and to interpret the photoelastic effect in terms of stress is called a polariscope. A standard crossed circular polariscope with the components arranged to provide a dark field in which the black isochromatics correspond to zero and integral orders was used in this investigation. The polariscope consisted of a monochromatic light source, collimating lens, polarizer, quarter wave plate, photoelastic model, quarter wave plate, analyzer, field lens, monochromatic filter, projection lens, and a viewing screen to which a Polaroid 4" x 5" film holder Model 500 was attached. The physical arrangement of these components was as shown in Figures IX and X.

The relationship between the optical effects and the stresses existing in a model may be obtained by analyzing the passage of light through a plane polariscope. Light from the source is plane-polarized by the polarizer, then revolved by the model into two components in the directions of the principal stress axes. When the principal stress intensities are not equal, the velocity of transmission on one principal stress plane will be different than on the other principal stress plane. This difference in velocities will cause a phase difference between the two component vibrations as they emerge from the model.

The phase difference is proportional to the difference of the principal stresses and is measured by introducing a

polarizing device called the analyzer. The analyzer brings part of each component vibration into interference in a single plane.

Consider a source of monochromatic light at normal incidence on a photoelastic model. When the monochromatic light has passed through the polarizer, the vibration is confined to a single plane in the direction of and with amplitude proportional to OA in Figure XI. This light may be represented by the equation:

$$S = a\cos(pt) \qquad (6)$$

where:

S - The Light Vector

a - The Amplitude of Vibration

p - Proportionality Factor of $2\pi f$

f - Frequency of Vibration

t - Time

When the light reaches the photoelastic model, its plane of vibration will usually not coincide with either principal plane of stress. Since the stressed model can only transmit light on the principal planes, the original vibration will be resolved into components as it enters the model. These components are:

$a\cos(pt)\cos\alpha$ Parallel to the No. 1 Principal Plane (7)

$a\cos(pt)\sin\alpha$ Parallel to the No. 2 Principal Plane (8)

where:

α - The Angle Between the Original Plane of Vibration and the No. 1 Principal Plane

If t_1 and t_2 are the times required for transmission on

the No. 1 and No. 2 principal planes respectively, then the two component vibrations leaving the photoelastic model will be:

$a\cos\alpha \cos p(t-t_1)$ Parallel to No. 1 Principal Plane (9)

$a\sin\alpha \cos p(t-t_2)$ Parallel to No. 2 Principal Plane (10)

The two vibration components leaving the model will have a phase difference, $p(t_1 - t_2)$ which can be shown to be proportional to the difference between the principal stresses. Let h represent the thickness of the photoelastic model along the path of light transmission, then:

$$t_1 = h/V_1 \quad \text{and} \quad t_2 = h/V_2 \qquad (11a,b)$$

then:

$$t_1 - t_2 = h\left(\frac{1}{V_1} - \frac{1}{V_2}\right) = h\left(\frac{V_2 - V_1}{V_1V_2}\right) \qquad (12)$$

Rewriting equation (5) as

$$C(\sigma_1 - \sigma_2) = V\ \frac{(V_2 - V_1)}{V_1V_2}$$

and combining with equation (12) we obtain

$$t_1 - t_2 = \frac{hC}{V}(\sigma_1 - \sigma_2) \qquad (13)$$

The phase difference, $p(t_1 - t_2)$, of the light waves leaving the model is seen to be directly proportional to the difference between the principal stresses $(\sigma_1 - \sigma_2)$. The phase difference is also proportional to the model thickness h and to the material and surrounding medium optical constant C/V.

By placing the analyzer in the proper position, the phase difference of the two waves can be determined by the interference effects of their components in the plane of the analyzer. When the plane of the analyzer transmission

is at right angles to the polarizer plane of transmission, the components of the two vibrations leaving the photoelastic model that will be transmitted by the analyzer will be given by the equations:

$$a\cos\alpha \sin\alpha \cos p(t-t_1) \qquad (14)$$

and

$$a\sin\alpha \cos\alpha \cos p(t-t_2) \qquad (15)$$

The two component vibrations lie in the same plane so they may be combined algebraically to give the following equation for the resultant vibration:

$$a\cos\alpha \sin\alpha \left[\cos p(t-t_1) - \cos p(t-t_2)\right] \qquad (16)$$

or

$$a\sin 2\alpha \sin p\left(\frac{t_1 - t_2}{2}\right) \sin p\left(t - \frac{t_1+t_2}{2}\right) \qquad (17)$$

Thus, the resultant vibration amplitude leaving the analyzer, equation (17), is a function of both the angle α and the phase difference $p(t_1 - t_2)$. So the resultant is affected by both the directions and the difference of the principal stresses at each point in the model.

The intensity of the light transmitted through any specific point in the photoelastic model is proportional to the square of the amplitude of vibration. A dark spot will occur on the model for every point at which:

$$a\sin 2\alpha \sin p\left(\frac{t_1 - t_2}{2}\right) = 0 \qquad (18)$$

The dark points are usually linked together to form loci representing one of two possible conditions:

(1) Isoclines - loci of constant principal stress direction (when α is zero or ninety degrees)

(2) Isochromatics - loci of constant principal stress difference, $(\sigma_1 - \sigma_2)$ (when $p(t_1 - t_2)/2$ is zero or $n\pi$ where n is an integer)

FIGURE IX

PHOTOGRAPHS OF POLARISCOPE

AND

ASSOCIATED APPARATUS

APR • 67

APR • 67

FIGURE X

SCHEMATIC DIAGRAM OF A STANDARD CROSSED CIRCULAR POLARISCOPE

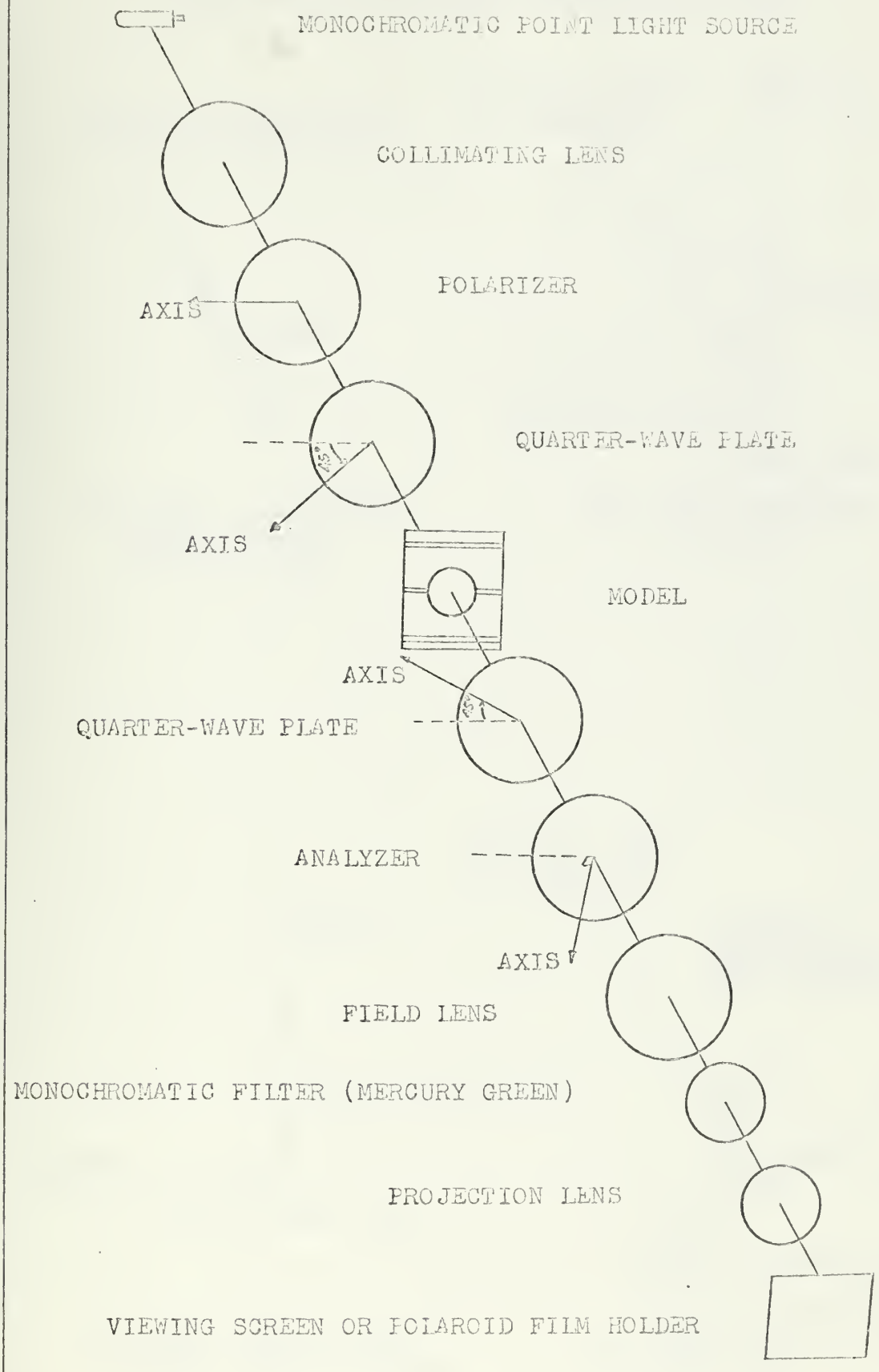

J.C.B. 1/3/67

FIGURE XI

LIGHT PATHS THROUGH A PLANE POLARISCOPE

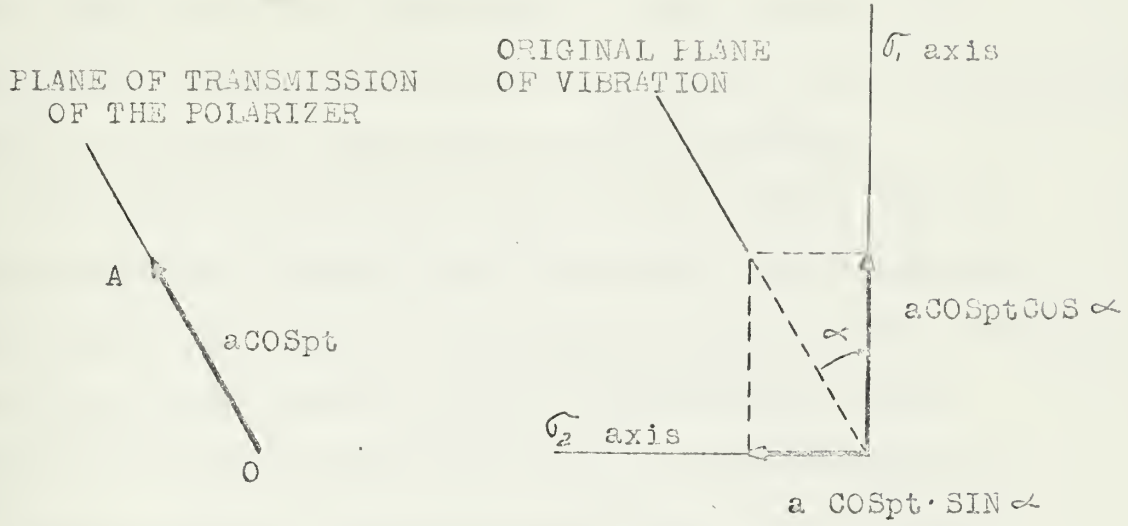

(a) PLANE - POLARIZED LIGHT LEAVING THE POLARIZER

(b) LIGHT ENTERING THE MODEL

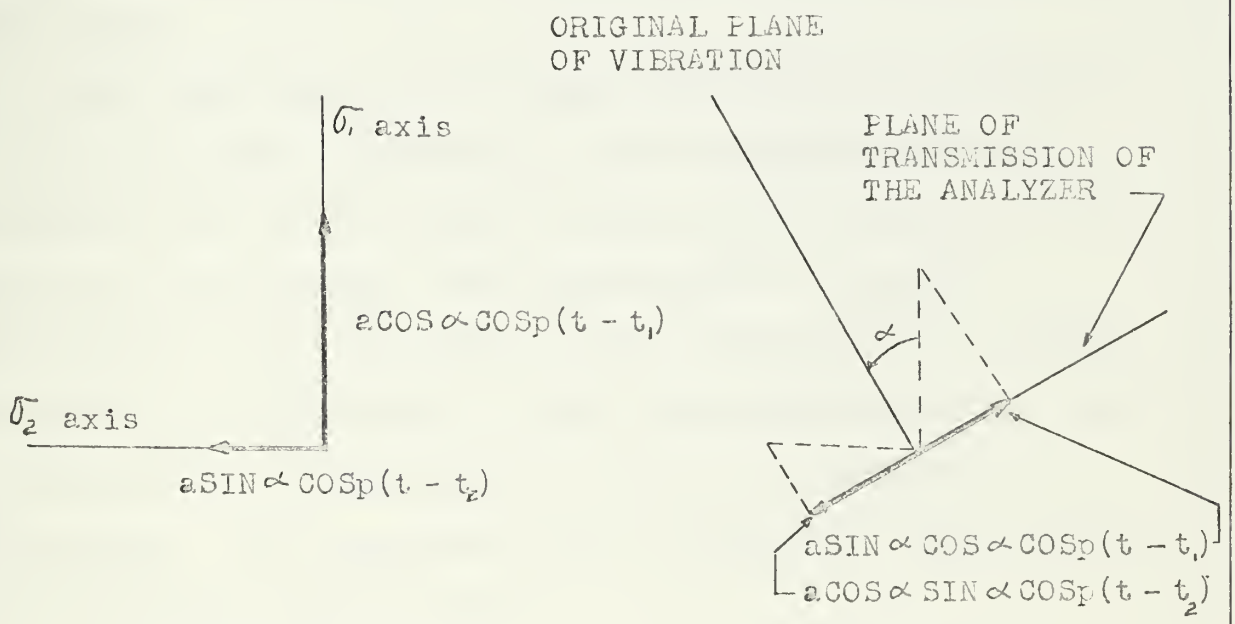

(c) LIGHT LEAVING THE MODEL (OUT OF PHASE)

(d) LIGHT LEAVING THE ANALYZER

dcb 1/3/67

In the plane polariscope, the isoclinic lines representing stress direction and the isochromatic lines representing stress magnitudes are superimposed on each other. In monochromatic light the combination of black lines representing these two different conditions may be confusing.

The addition of the two quarter-wave plates to the plane polariscope converts the instrument into a circular polariscope. The quarter wave plates eliminate the isoclines, so that the image consists only of isochromatic lines representing stress magnitudes alone. The light beam is now circular rather than plane polarized. In selecting the quarter wave plates it is more important that they match each other than that they correspond exactly to one quarter of the wave length of the monochromatic light being used. If the deviation is the same for both plates, there will be no error if they are in opposition because the error produced by the first is removed by the second quarter wave plate.

This investigation has been conducted with a standard crossed circular polariscope. The photography has been conducted with a dark field in which the quarter wave plate axes are also crossed. With monochromatic light the isochromatic lines are shown as dark bands known as fringes or orders of interference. Each fringe represents the locus of all points having a constant value of principal stress difference. This condition can be represented mathmatically by rearranging equation (13):

$$t_1 - t_2 = \frac{hC}{V} (\sigma_1 - \sigma_2)$$

or $$(\sigma_1 - \sigma_2) = \frac{V}{Ch} (t_1 - t_2) = \frac{fn}{h} \qquad (19)$$

where:

f - Fringe Constant of the Photoelastic Material with Units of (lbs/inch/order)

n - Order of Interference

h - Thickness of the Photoelastic Model

Materials utilized in photoelastic stress analysis display a linear variation between the optical retardation effects and stress magnitude. The change in the difference of stresses from one order of interference will be a constant.

The zero order of reference must be determined by observing the fringe pattern grow as the load is applied to the model. A zero order or point of zero stress remains dark at all times and is used as a reference in interpreting the stress pattern. For the purposes of fringe order determination, the stress patterns are divided into two types: the simple and the complex. A simple stress pattern is one in which the fringe of zero order is retained regardless of the magnitude of the loads. A stress pattern in which the fringe of zero order disappears is of the complex type. With the geometry of the models in this experiment it was necessary to observe the sources and the general growth of the patterns as the load was applied to fix a reference order point. On most of the models the readily observable zero order regions moved off the model.

3. The Polariscope Alignment and Use

The actual alignment of the polariscope consisted of several steps. The long and the short optical benches were aligned by carefully laying out the benches on their respective tables and then the tables with respect to the laboratory wall. A tightly stretched thread served as a check on the alignment. All components were placed on the optical benches as shown in Figures IX and X such that the guide ball bearings were all on the same side of the tracks. The polarizer and analyzer assemblies were positioned as close to the model as possible. The condensing lenses convex side should be towards the model. The collimating lens and light source spacing was adjusted so that reflected light rays formed as small a point as possible (size of light hole) on the light source housing. The spacing between the field lens and the monochromatic filter was adjusted so that a small image appeared on the center of the filter. The smaller aperture in the light housing was used for all photography.

A special plywood adaptor plate was made for the polariscope camera that permitted the use of a portion of the camera attachment and Polaroid Film Holder Model 500. This photographic equipment was obtained from the Experimental Stress Analysis Laboratory of the Mechanical Engineering Department as part of the Photolastic Inc. Model 051 Transmission Polariscope.

The film used was Polaroid Type 55 P/N. This provides

both a positive and a negative. The negative was projected on a screen to facilitate counting the fringes accurately. The exposure time was about two to four seconds with the small point mercury green source.

4. The Free Boundary Effect

The general expression for obtaining the differences of the principal stresses at any point in a loaded photoelastic model is equation (19):

$$\sigma_1 - \sigma_2 = \frac{fn}{h} \qquad (19)$$

At a free boundary, for reasons of equilibrium, only one principal stress is present, and it has to be in the tangential direction so that equation (19) becomes

$$\sigma_t = \pm \frac{fn}{h} \qquad (20)$$

and

$$\sigma_n = 0 \qquad (21)$$

where:

σ_t - The Magnitude of the Tangential Stress

σ_n - The Magnitude of the Normal Stress

The plus or minus signs are introduced because the tangential stress can be either tensile or compressive.

In determining the sign of the stresses around a free boundary we can observe that the nature of the stress around a boundary remains the same as long as the isochromatic or fringe lines remain essentially parallel to each other. The sign of the stress at a point can be determined by inspecting the geometry of the model and observing the manner in which it is loaded. Around an

interior free circular boundary, we can expect to find four isotropic points of zero order due to the geometries involved in the model and its loading. These points will serve to separate the two tensile and two compressive regions on the interior circumference.

B. DETAILS OF PROCEDURE

1. General

In this investigation, the region of interest is the circular reinforced free boundary. Relating the weight or volume of material, the reinforcement geometry, and the efficient utilization of material was done through the Stress Concentration Factors. This Stress Concentration Factor is the ratio between the maximum and minimum stresses that occur on the circular free boundary.

These stresses are determined by the equation

$$\sigma_t = \pm \frac{fn}{h} \qquad (20)$$

as previously given.

2. Preparation and Construction of the Models

The general configuration of the seventeen models used in this investigation are described in Table I.

The geometries involved in the components of these models was such that several steps were needed to arrive at the final shapes of the photoelastic material.

For the circular and two elliptical reinforcements and their individual curved frame appendages three steps were followed in obtaining these parts. First a template three times the desired final size of each of these six shapes was made from three-eights inch thick plywood. The plywood templates were rough cut to size in the Ship Model Shop and then sanded to the exact size. These plywood templates

were then used as the guide pattern on a pantograph in a Metallurgy Department Machine Shop. To be compatable with the desired three to one size reduction ratio a 1/8 inch end-mill and a 3/8 inch guide pin were used. On the pantograph, templates the same size as the desired finished photoelastic material parts were machined from 0.10 inch thick sheet aluminum. These aluminum templates were then smoothed using a fine gunsmith checkering tool file and carborundum watersand paper of 400 grit. These aluminum templates now served as the guides for cutting of the photoelastic material.

The sheet PS-5 material was rough cut to within approximately 1/16 inch of the final desired dimensions as traced on the protecting paper coverings. The small jig saw in the Ship Model Shop was used with an ultra fine blade obtained from the Ship's Structures Laboratory. Then the Chapman High Speed Tungsten Carbide Cutter in the Ship's Structures Laboratory was used for the final machining of the PS-5 components.

The rough cut PS-5 components were attached to the aluminum templates using double sided masking tape. The roughing guide was inserted into the high speed cutter and the parts machined to within 0.007 inch of their final dimensions. The finishing guide was then inserted and the models cut to their final size. PS-5 material is not as susceptible to chipping and the development of edge stresses as some other materials. Care is required in machining small parts since the cutter is turning at 45,000 rpm and small

cuts must be taken to avoid grabbing of the cutter.

The parts were then separated from the templates and inspected under 10X magnification on the Transmission Polariscope in the Experimental Stress Analysis Laboratory for edge stresses. No edge stresses were noted which indicated that the high speed cutter was being used with light enough cuts.

In all a total of fifty one different photoelastic parts were machined exclusive of the two calibration disks. These parts consisted of five four inch square foundation pieces, sixteen reinforcing frames of 3/8 x 1/4 x 4 inches, six circular reinforcements of two inch outside diameter, six elliptical reinforcements with a major axis of two and one half inches and a minor axis of two inches, six elliptical reinforcements with a major axis of three inches and a minor axis of two inches, and three sets of four appendages each to fit the contours of the circular and elliptical reinforcement pieces. The fillet radius of these appendages was two inches. All foundation pieces and circular and elliptical reinforcements were center bored to one and one quarter inch diameter.

A wooden jig was then constructed which would aid in the alignment of the components to be attached to each side of the three main foundation pieces. This consisted of cavities for each of the parts such that two ribs and the two contoured appendages on each side could be cemented and held in alignment while the cement set.

The cement was Photolastic, Inc. PC-1 (Clear) with hardener PCH-1. This resin cement matches the properties of

the sheet materials. It requires twelve hours to cure. Great care is required in measuring out the two ingredients so as to maintain the proper relationship of ten parts hardener to one hundred parts of the PC-1 resin. To assist in the accurate mixing, a Redding Powder and Bullet handloading scale was utilized. This scale is guaranteed accurate to one tenth grain. Very small amounts of cement were mixed as it should be used sparingly and only a few parts joined at one time. A polished aluminum dowel pin was made to aid in the alignment of the reinforcement holes.

Even with extensive care in machining and alignment, there are visible differences in certain areas on the models. These differences are probably the cause of some symmetry problems incurred while loading the models.

3. Model Configuration

The general configuration of each of the models is as described in the following table.

TABLE I

BASIC MODEL DESCRIPTION

MODEL NUMBER	CONFIGURATION
1	Unreinforced Foundation Piece
2	Reinforced with Rib Frames on Outside Edges
3	Reinforced with One 0.080" Circular Reinforcement on Each Side
4	Reinforced with One 0.080" Small Ellipse on Each Side
5	Reinforced with One 0.080" Large Ellipse on Each Side
6	Reinforced with Three Circular Reinforcements
7	Reinforced with Three Small Ellipses
8	Reinforced with Three Large Ellipses
9	Reinforced with Four Circular Reinforcements
10	Reinforced with Four Small Ellipses
11	Reinforced with Four Large Ellipses
12	Reinforced with Five Circular Reinforcements
13	Reinforced with Five Small Ellipses
14	Reinforced with Five Large Ellipses
15	Reinforced with Six Circular Reinforcements
16	Reinforced with Six Small Ellipses
17	Reinforced with Six Large Ellipses

Note: Models 3 through 17 all have the frame ribs on two outside edges and the appropriate contoured pieces to fit against the particular circular or elliptical reinforcements on the holes.

4. Loading

In an ideal model in which the material distribution is perfectly symmetrical, a uniform edge compressive load would result in a perfectly symmetrical fringe pattern in all four quadrants. This perfect symmetry of material and loading is rather difficult to attain. By the use of carefully constructed wooden jigs for the cementing process, it was hoped to attain accurate joining of the various reinforcing components to the basic foundation piece. Then, by the use of a piece of small (one quarter inch diameter) round stock, the bearing point of the load cell on the upper loading frame piece could be adjusted so that the fringe pattern on either side of a vertical line down through the center of the model could be made symmetrical. This was the ideal pattern desired. The attainment of this was very difficult and time consuming due to the high sensitivity of the fringe pattern to the position of the round stock under the load cell.

Any lack of symmetry above and below a horizontal line through the center of the model proved to be incapable of correction. There was no means of adjusting the free boundary on the sides to aid in attaining symmetry of the fringe pattern.

As a means of obtaining the best approximation to a uniformly distributed load along the edges under compression, this load was transmitted through a layer of several sheets of thin cardboard. The reason for the cardboard spacers between the photoelastic model and the loading frame pieces

is related to the boundary conditions desired. The distribution of the stresses in pieces of rectangular form when loaded partially in compression depends upon the boundary conditions. Even if the two surfaces being loaded in compression are perfectly plane, the distribution of the stresses will not be uniform. Under compression the width of the photoelastic model is increased by about one third of the length contraction. On the surface of contact, the friction with the aluminum loading frame does not allow the expansion of the photoelastic material. This would introduce a lateral compression on the boundary.

The best way to obtain a uniform, or nearly uniform distribution of the stresses in the model, is to introduce a material which does not develop tangential stresses and does equalize the normal stresses. These conditions appear to be realized by using cardboard spacers. The effect of the cardboard is to allow a freer expansion of the boundary.

In addition to aiding with the poisson effect problems, the cardboard spacers probably also help to distribute the load more uniformly. When the loading was applied along the edges at right angles to the framing direction, each bearing edge was composed of seven different pieces in the built up models. Any slight deviation from a perfectly uniform edge alignment when cementing the pieces together may be somewhat compensated for by the cardboard spacers. The loading frame that held the models consisted of two identical top and bottom pieces and two alignment rods as shown in Figure XII.

FIGURE XII

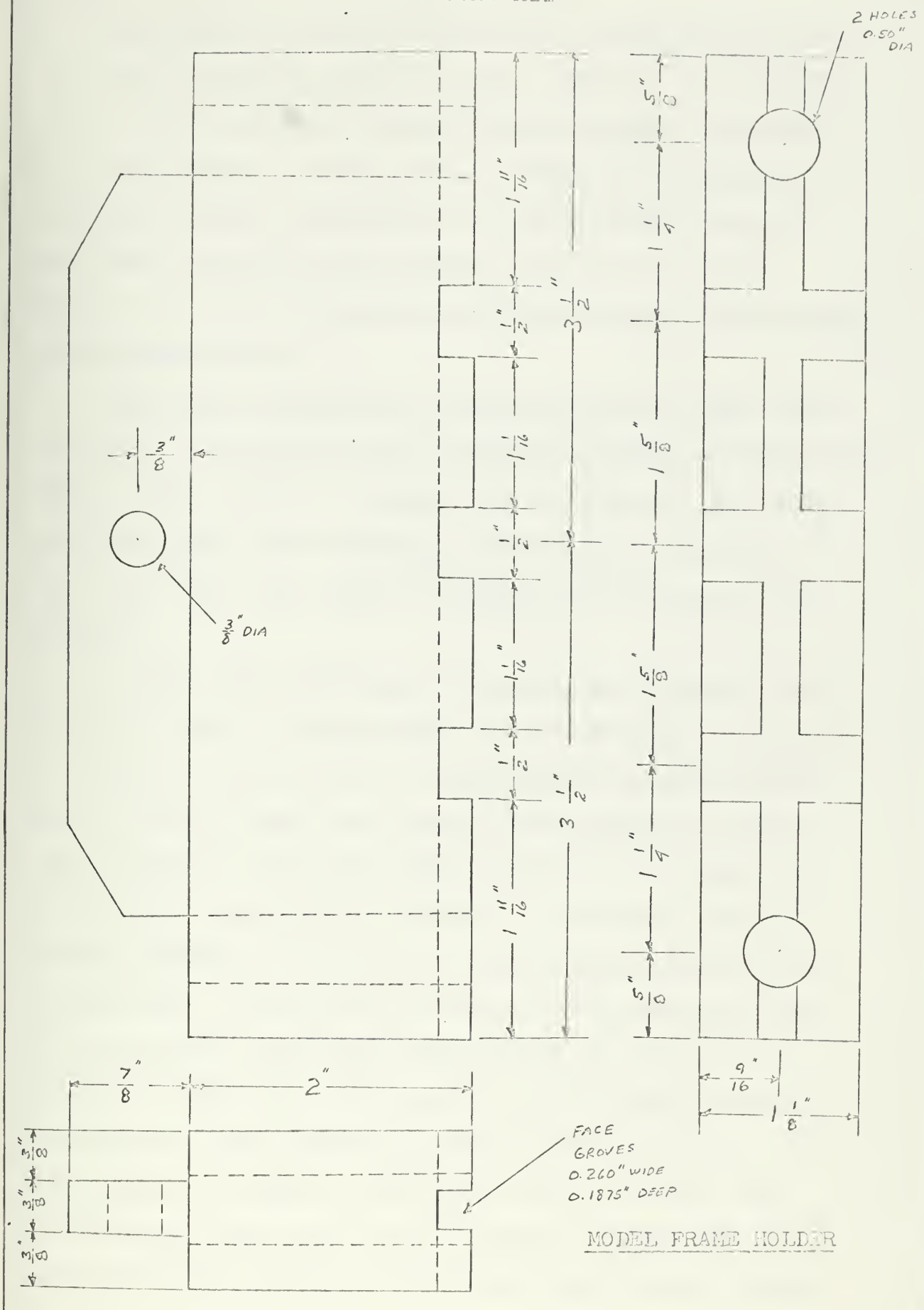

MODEL FRAME HOLDER

JCB 7/3/67

To attain a perfectly symmetrical fringe pattern with all these potential sources of non-uniformity was difficult. In the final analysis, the most uniform pattern attainable with adjustments to the point of loading was photographed. Then the average fringe order of both vertical and both horizontal free circular boundary points were used to obtain the stress concentration factor between the horizontal and vertical axes.

Buckling considerations would serve as an upper limit to which a photoelastic model should be loaded in compression. When a model started to buckle, the curvature of the model surfaces which were originally normal to the direction of the light beam would tend to degrade the accuracy of the results.

In this investigation, it was desired to load a model along the edges at right angles to the direction of framing to represent hoop stress in a cylindrical pressure vessel wall. Then the model was turned ninety degrees so that the loading was along the edges parallel to the direction of framing. The load was reduced to a value to produce an edge loading of one half the force applied for the hoop loading case. This reduced loading on the other two edges is to represent the longitudinal stress in a cylindrical pressure vessel wall. The ratio of two to one is strictly valid for an unstiffened cylindrical pressure vessel. As ring frames are added, these would tend to relieve some of the hoop stress level in the pressure vessel wall but only have local effects on the longitudinal stress levels.

These square photoelastic models can be thought of as an element cut from a pressure vessel. The force balance to maintain this element in equilibrium will remain the same as ring frames are added. The loading was therefore maintained at a simulated two to one force balance on the photoelastic model.

5. Load Cell Calibration

The load cell available for this investigation was manufactured by the Baldwin-Lima-Hamilton Corporation. Since the exterior name plate data was not available, the problem became one of calibrating an unknown universal load cell. By the physical dimensions it was estimated to be of about a ten thousand pound capacity and of World War II vintage. The color coded wiring established its identity as a BLH product with a full wheatstone bridge.

After several initial trial gage factor settings on a Budd Strain Indicator, the value of 0.60 gage factor was determined to give a one to one relationship between microstrain and pounds.

By the use of a mechanical balance with two pound increments in loading, the linearity of the load cell was checked up to a five thousand pound loading.

LOAD CELL

Manufacturer: BALDWIN-LIMA-HAMILTON CORPORATION
Serial Number 5019
Estimated Capacity: 0-10,000 lbs Tension or Compression

STRAIN INDICATOR

Manufacturer: BUDD COMPANY
Serial Number 1895
Model P-350
Gage Factor Setting 0.60

BALANCE

Manufacturer: RIEHLE BROS.
Serial Number 17079
Range: 0-10,000 lbs in 2 lb Increments

TABLE II

LOAD CELL CALIBRATION DATA

Instrument Reading $\mu\epsilon$	Increment $\mu\epsilon$	Compressive Load lbs.
+ 2909	0	0
+ 2889	20	20
+ 2869	40	40
+ 2849	60	60
+ 2829	80	80
+ 2809	100	100
+ 2701	208	200
+ 2601	308	300
+ 2500	409	400
+ 2400	509	500
+ 2292	617	600
+ 2198	711	700
+ 2090	819	800
+ 1993	916	900
+ 1891	1018	1000
+ 1390	1519	1500
+ 883	2026	2000
+ 382	2527	2500
- 120	3029	3000
- 615	3524	3500
- 1100	4009	4000
- 1609	4518	4500
- 2108	5017	5000

FIGURE XIII

LOAD CELL/STRAIN INDICATOR CIRCUIT

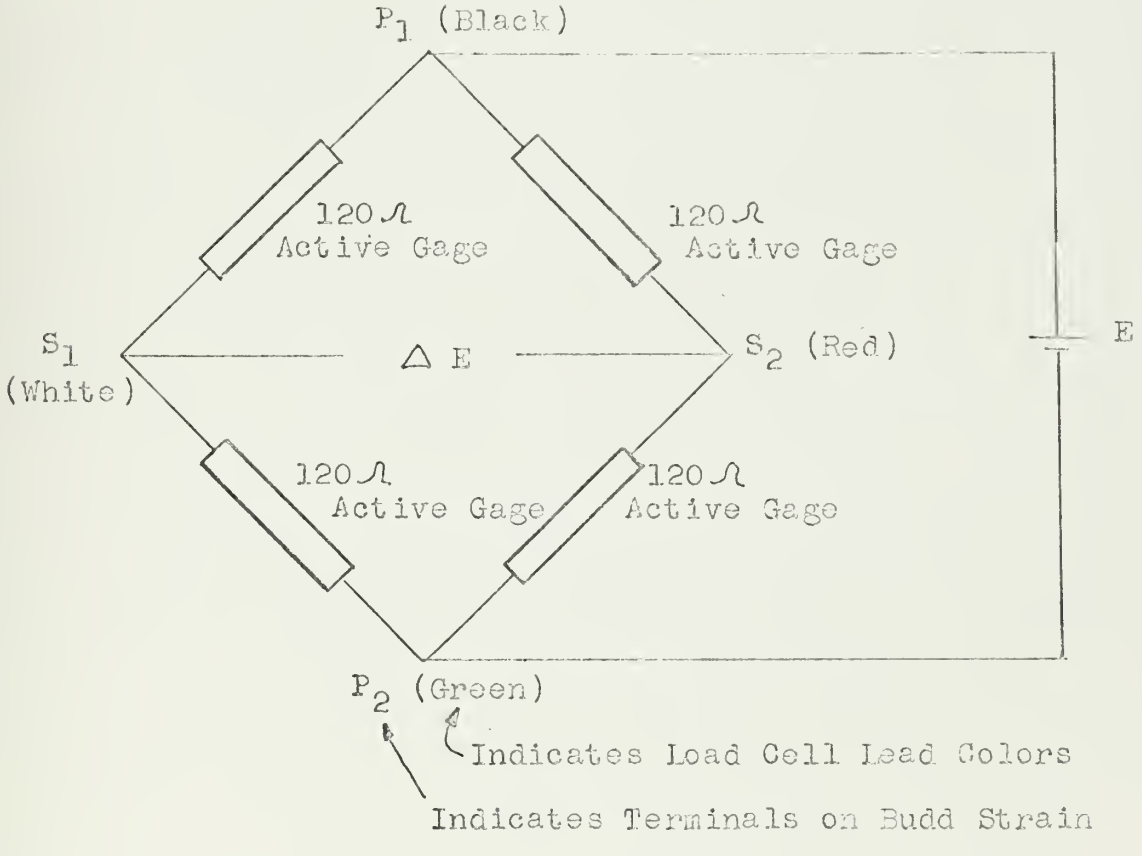

Full Wheatstone Bridge Load Cell

(Four Active Gages)

Sensitivity of Load Cell is 0.60 μinch/inch per lb.

JCB 13/4/67

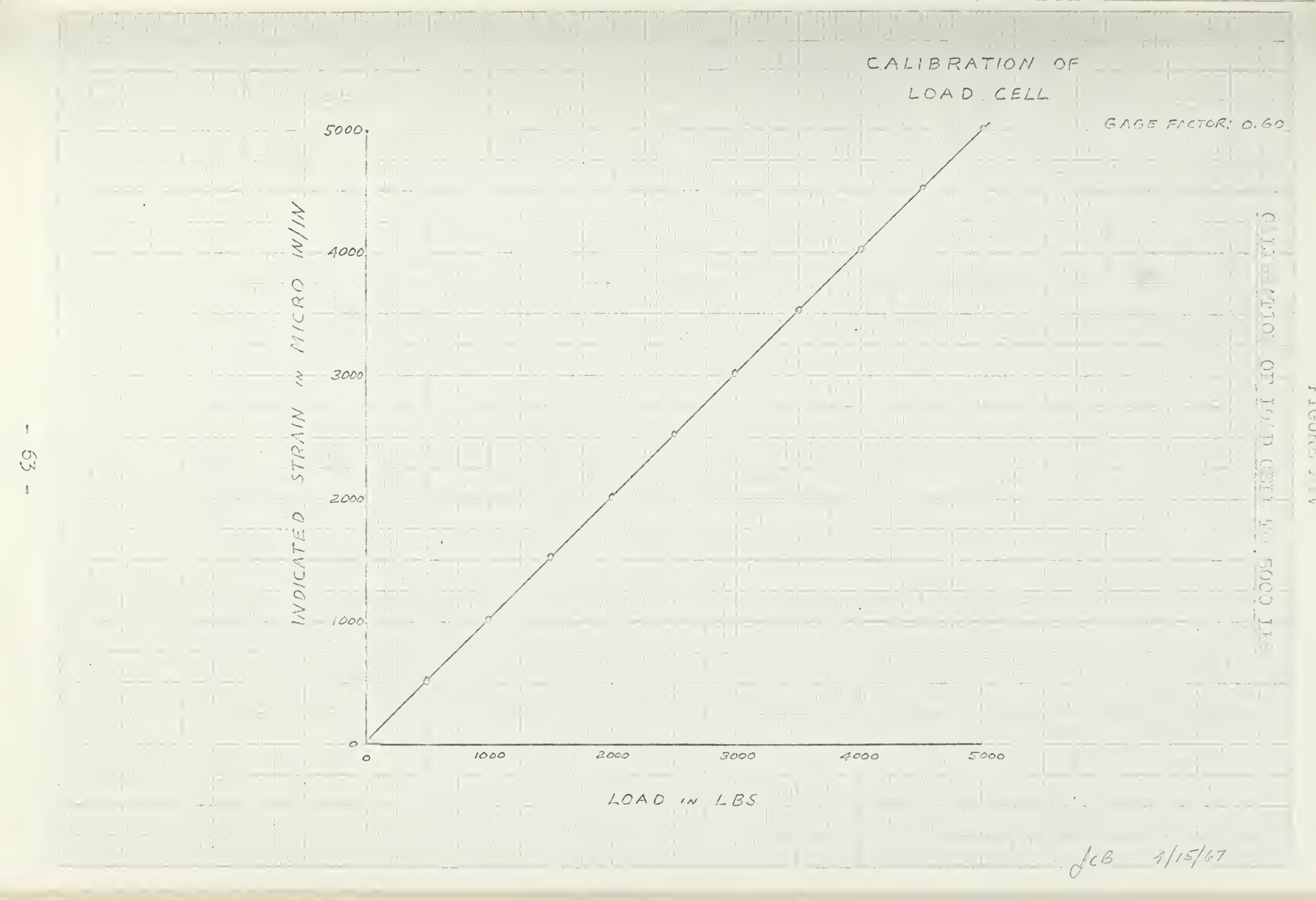
CALIBRATION OF
LOAD CELL
GAGE FACTOR: 0.60
INDICATED STRAIN IN MICRO IN/IN
5000
4000
3000
2000
1000
0
0
1000
2000
3000
4000
5000
LOAD IN LBS
JCB 1/15/67

CALIBRATION OF LOAD CELL

GAGE FACTOR: 0.60

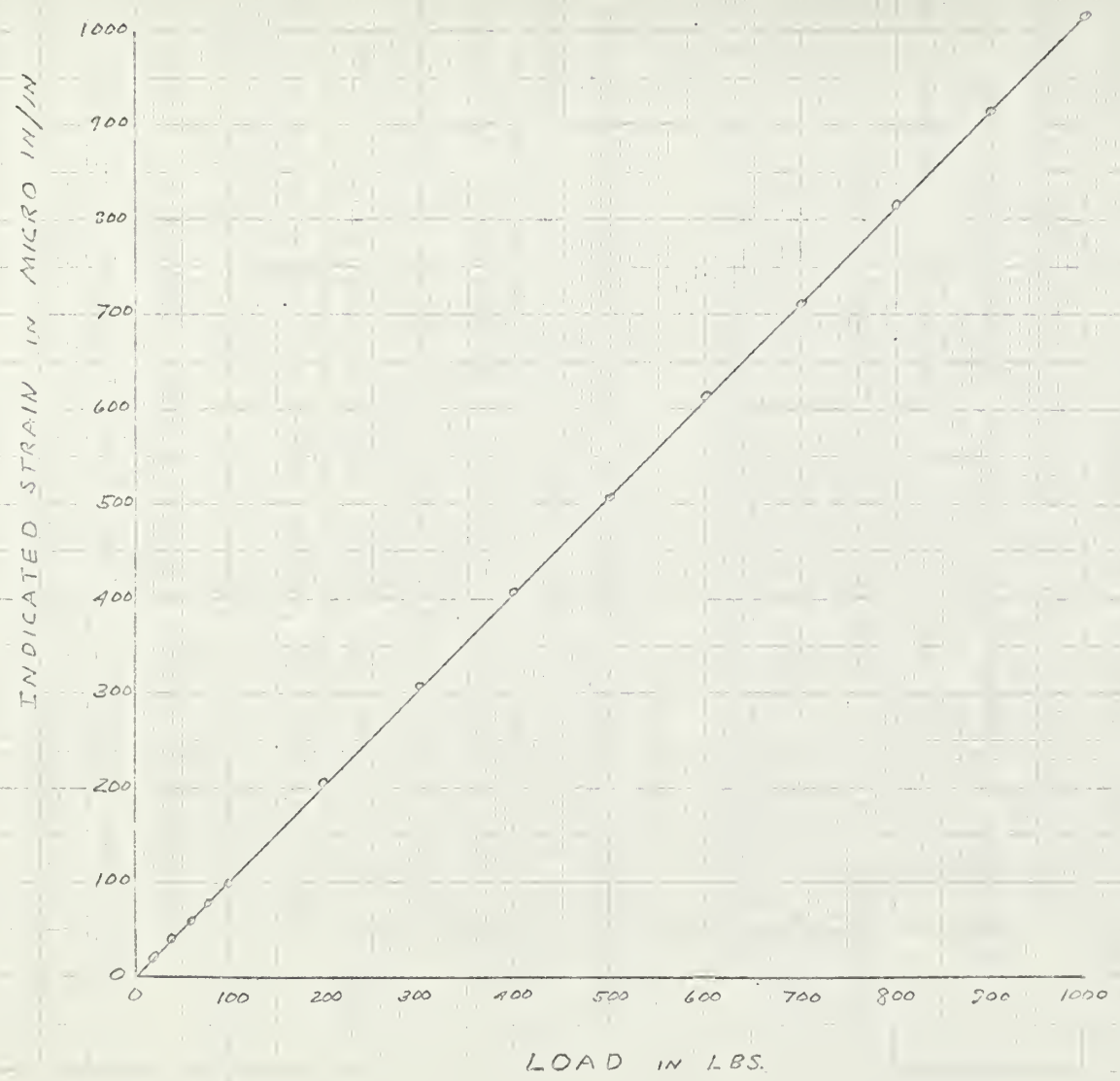

JCB 1/15/67

6. Determination of the Fringe Order

This series of investigations was conducted using a monochromatic light source. With the standard crossed circular polariscope the axes of the polarizer and analyzer are crossed and the fast axes of the one quarter wave plates are crossed so as to be in opposition to one another. This configuration presents a dark field in which the dark lines in the isochromatic pattern correspond to zero and integral orders. By merely rotating the axis of the analyzer by ninety degrees so that the axes of the polarizer and analyzer are parallel we obtain a light field in which the dark lines in the isochromatic pattern correspond to half orders.

The fringe order at any particular point is determined by locating a point of zero order and counting the fringe lines crossed in reaching the point of interest. The zero fringe is located by the fact that its position remains fixed under all loading levels. With the dark field of the standard crossed circular polariscope, the entire model is dark when unloaded. That is, the zero order covers the model. As the model is loaded, only the zero order points will remain dark and fixed under all loads. All the remaining portions of the model will alternately be dark or light as the loading level is changed.

The points of zero order were obtained by observing the initial loading of the model and by inspecting the geometric fringe patterns around the free inner boundary. There are

four points of zero order or isotropic points on the inner free surface that represent the points where the tangential boundary stress changes from a tensile to a compressive stress. An observation of the loaded model can also be made with white light to establish which of the fringes belong to the zero order since this order will always appear black.

By the process of shifting from a dark field to a light field, both the integral and half orders can be observed. Thereby, the accuracy of fractional order estimates may approach one quarter order. The method of plotting the integral fringe orders versus angular position around the inner free boundary also will permit a more accurate estimate of the fractional order at any point on the boundary. This latter method has been utilized for model one and two. Both the hoop stress and the longitudinal stress components have been plotted in this manner and then the stresses have been superimposed.

7. Properties of PS-5

The photoelastic material used in this investigation was manufactured by Photolastic, Inc. of Malvern, Pennsylvania. The accuracy of the model technique depends upon the quality and reliability of the model material. The recent materials developed by Photolastic, Inc. give consistent sheets that are free of internal stress, have excellent transparency, very low time-edge effect and high sensitivity. For the

fabrication of built up models, adhesives are available which match the properties of the component parts. Careful quality control assures that sheet properties are uniform from lot to lot.

PS-5 material is an epoxy synthetic resin with the following properties listed by the manufacturer:

Modulus of Elasticity (E)	450,000 psi
Poisson's Ratio (ν)	0.36
Stress Optical Constant	60 psi/fringe/inch

The estimated tensile strength is 9,000 psi, with the yield strength above 3,000 psi. The PS-5 material is about twice as expensive as the older CR-39 material, but the very uniform qualities of the PS-5 material make it better suited to detailed photoelastic analysis.

8. Determination of the Material's Fringe Constant

The necessity of determining the quantitative significance of the isochromatic fringe pattern in terms of stress levels is required for any problem in which absolute stress values, rather than relative values, are needed. Evaluation of the fringe constant "f" is a determination of the stress-optic constant of the material.

The fringe constant represents the change in the difference between the principal stresses that will produce a change of one order of interference at a given point in a piece of material having a unit thickness.

The fringe constant depends on the type of material and

may vary from one lot to another such that it is necessary to check the calibration each time a new lot is used. The fringe constant also depends on the wave length of the light being used in the experiment.

The fringe constant was determined for two monochromatic light sources. The normal monochromatic light available with the Polarizing Instrument Company polariscope in the Ship's Structures Laboratory is mercury green with a wavelength of 5461 angstroms. This wavelength was obtained by using a mercury lamp as a light source and a mercury green filter. To allow for the possible use of the Photolastic Inc. Transmission Polariscope Model 051 with 10X magnification in the Mechanical Engineering Department's Experimental Stress Analysis Laboratory, the fringe constant for sodium yellow light was also determined. This wavelength corresponds to the tint of passage at 5893 angstroms.

In any calibration technique one must select a geometrical shape and loading for which the theoretical stress distribution is accurately known. Among the common calibration specimens are tensile bars, beams under pure bending, and circular disks under diametral loading.

For several reasons a circular disk was selected as the calibration geometry. Among the reasons were that the compressive loading of the disk represents the type of loading to be utilized throughout the experiments so the loading apparatus was used in a consistent fashion, the ease of machining, and that the principal stresses at the disk center are known from the theory of elasticity.

The fringe order n_c at the center of the disk can easily be observed with a high degree of precision. It is not materially affected by any initial edge stresses. Therefore the disk provides a simple and accurate means of determining the fringe constant of the material in a compressive load application.

From the theory of elasticity for the case of a disk, the stresses along the horizontal diameter are given by:

$$\sigma_x = \sigma_1 = \frac{2P}{\pi hD}\left[\frac{D^2 - 4x^2}{D^2 + 4x^2}\right]^2 \qquad (22)$$

$$\sigma_y = \sigma_2 = -\frac{2P}{\pi hD}\left[\frac{4D^4}{(D^2 + 4x^2)^2} - 1\right] \qquad (23)$$

$$\tau_{xy} = 0 \qquad (24)$$

at the center of the disk $x = 0$ so these reduce to:

$$\sigma_1 = \frac{2P}{\pi hD} \quad \text{and} \quad \sigma_2 = -\frac{6P}{\pi hD} \qquad (25\ a,b)$$

Then: $\sigma_1 - \sigma_2 = \frac{8P}{\pi hD} = n_c \frac{f}{h}$

Therefore:

$$f = \frac{8P}{\pi D n_c} \qquad (26)$$

The fringe order n_c is a linear function of (P/D) and is independent of the thickness of the material.

Two compressive disks from one quarter inch thick material of the same lot number as the models were used for calibration purposes. These disks were machined to diameters of 2.710 inches and 2.395 inches.

A disk was loaded in compression and the load recorded at which each integral order of interference reached the center of the disk. After reaching the eighth order the

disk was slowly unloaded and the loads recorded at which the fringes at the center were reobtained. This procedure was repeated several times with both mercury light and sodium yellow monochromatic light. Since mercury light was used through out the investigation, only these results are included in Figure XVI.

The slope of the load P/D versus fringe order n_c curve was obtained from the graphs. The fringe constant was calculated using equation (26):

$$f = \frac{8P}{\pi D n_c} \qquad (26)$$

where:

f - Fringe Constant of the Material (lbs/in/order)

P/n_c - Slope of the P versus n_c curve (lbs/order)

P - Diametral Load on the Disk (lbs)

n - Order of Interference

D - Diameter of the Disk (inches)

Further loading of the disk would not improve the accuracy of the fringe constant since the assumption of point diametral loading becomes less valid as the disk is flattened at the points of load application.

TABLE III

FRINGE CONSTANT CALIBRATION READINGS

Monochromatic Light: Mercury Green - Wavelength 5461 Angstroms

Disk Diameter: 2.710 inches

Fringe Order at Center n_o	Strain Indicator Readings (μ in/in) Increasing Load	Decreasing Load	Average Load	Avg Load Diameter
0	0 lbs	0 lbs	0 lbs	0 lbs/in
1	49	45	47	17.3
2	108	96	102	37.6
3	166	154	160	59.6
4	228	225	226.5	83.6
5	286	270	278	102.6
6	345	333	339	125.1
7	403	385	394	145.4
8	464	464	464	171.2

Disk Diameter: 2.395 inches

0	0 lbs	0 lbs	0 lbs	0 lbs/in
1	43	40	41.5	17.3
2	87	78	82.5	34.5
3	144	140	142	59.3
4	193	181	187	78.1
5	241	245	243	101.5
6	295	296	295.5	123.4
7	346	341	343.5	143.4
8	397	397	397	165.8

TABLE IV

FRINGE CONSTANT CALCULATIONS

Average Load/Diameter Ratios for Both Disks vs n_c

Fringe Order (n_c)	Mercury Green Light	Sodium Yellow Light
0	0 (P/D)	0 (P/D)
1	17.3	19.1
2	36.1	41.2
3	59.2	62.0
4	80.7	85.8
5	102.0	108.9
6	124.3	128.5
7	144.4	153.8
8	168.5	177.5

Plotting of mercury green values in Figure XVI gives the slope of the n_c vs P/D relationship. Sodium yellow graph is not included in this thesis but the fringe constant is given below.

Mercury Green

$$f = \frac{8P}{\pi n_c D} = \frac{8}{\pi}\left(\frac{\Delta P}{D}\right)\left(\frac{1}{\Delta n_c}\right) = \frac{8}{\pi}(167-17)\frac{1}{(8-1)} = 54.6$$

Average Fringe Constant: 54.6 lbs/in/order

Sodium Yellow

$$f = \frac{8P}{\pi n_c D} = \frac{8}{\pi}(175-18.5)\left(\frac{1}{8-1}\right) = 57.0$$

Average Fringe Constant: 57.0 lbs/in/order

DETERMINATION OF FRINGE CONSTANT

MONOCHROMATIC LIGHT:

MERCURY GREEN

5461 Å

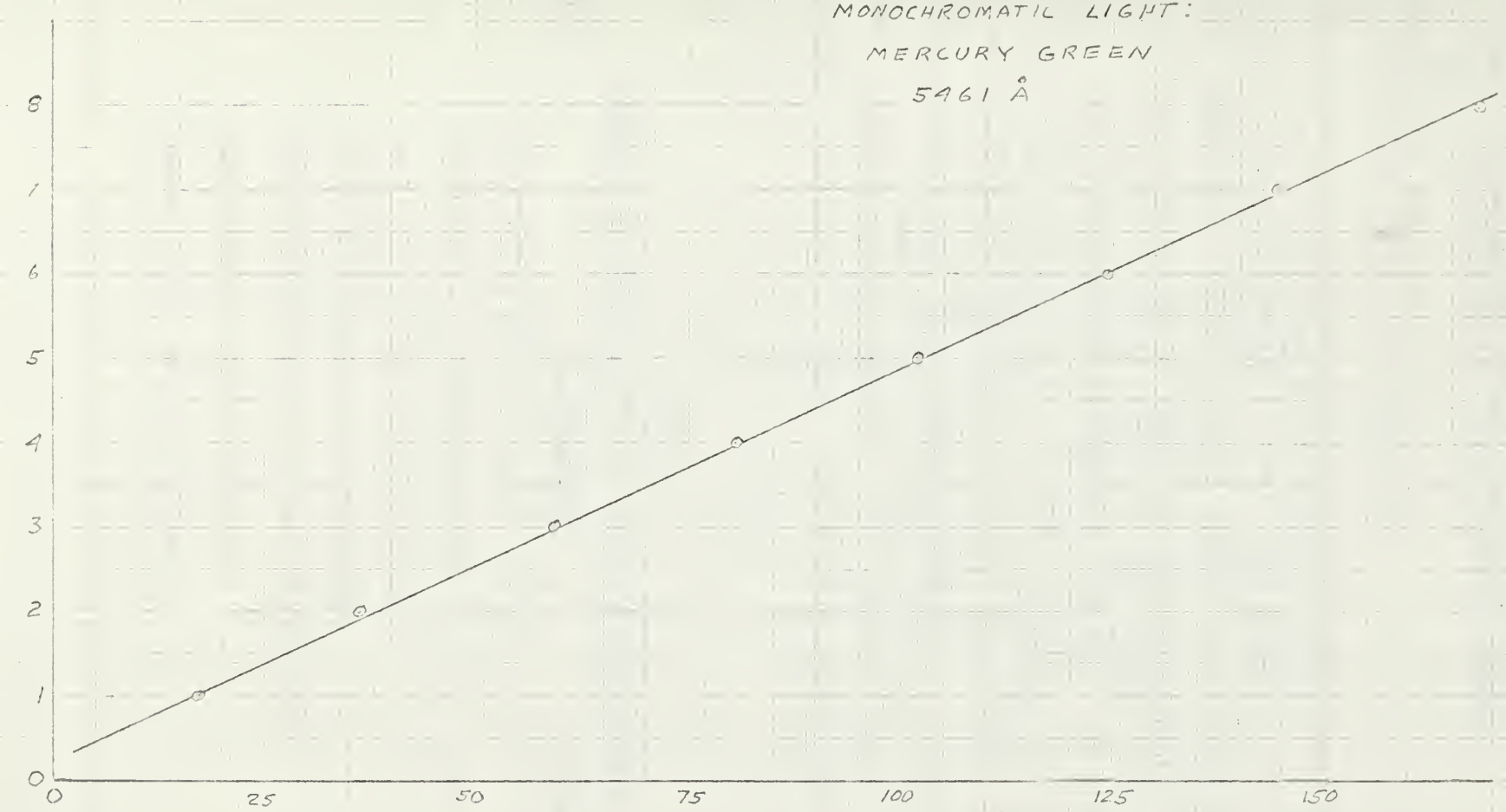

RATIO: $\frac{\text{LOAD}}{\text{DIAMETER}} = \frac{P}{D}$ $\frac{\text{LBS}}{\text{INCH}}$

FIGURE XVI

JCB 2/15/67

C. SUMMARY OF DATA AND CALCULATIONS

1. Geometry and Weights of Components

The density of PS-5 material is about 317 grains per cubic inch where 7,000 grains equals one pound.

The weight and volume of some shapes is as follows:

Circular hole in base piece volume is $\frac{\pi(1.25)^2}{4}(0.245) = 0.305$ in^3

Circular hole in base piece weight is (317)(0.305) = 96.6 grains

Ring frame reinforcement strip is 3/8 x 4 x (0.245) = 0.368 in^3

Weight of two full reinforcement strips 2 x (0.368) x 317 = 233.6 gr.

Total removed material from models 2 through 17 is 330.2 grains

Total material removed to obtain a bare base piece is 797.4 grains. This includes six full length frame strips and the center hole.

TABLE V

WEIGHTS OF COMPONENTS TO MAKE UP THE MODELS

Item No.	Discription	Weight in Grains
1	Ring Frame Reinforcement Strip	116.8
2	Circular Disk Reinforcement (0.080" thick)	45.3
3	Small Elliptical Reinforcement	65.3
4	Large Elliptical Reinforcement	83.3
5	Supports For Circular Reinforcements	35.0
6	Supports For Small Ellipse	27.0
7	Supports For Large Ellipse	20.0

Model numbers 2 through 17 all have two reinforcing strips on each side near the outside edge to represent ring frames.

The following table shows the manner in which the reinforcement weights have been added.

TABLE VI

WEIGHTS OF MODEL REINFORCEMENTS

Model No.	Reinforcements	Column 1	Column 2	Column 3
1	Foundation Piece Alone	0	-	-
2	Four Edge Strips Added	467.2	-	-
3	Two Circular Reinforcements	697.8	0	0
4	Two Small Ellipses	705.8	0	8.0
5	Two Large Ellipses	713.8	0	16.0
6	Three Circular Reinforcements	743.1	45.3	45.3
7	Three Small Ellipses	771.1	65.3	73.3
8	Three Large Ellipses	797.1	83.3	99.3
9	Four Circular Reinforcements	788.4	90.6	90.6
10	Four Small Ellipses	836.4	130.6	138.6
11	Four Large Ellipses	880.4	166.6	182.6
12	Five Circular Reinforcements	833.7	135.9	135.9
13	Five Small Ellipses	901.7	195.9	203.9
14	Five Large Ellipses	963.7	249.9	265.9
15	Six Circular Reinforcements	879.0	181.2	181.2
16	Six Small Ellipses	967.0	261.2	269.2
17	Six Large Ellipses	1047.0	333.2	349.2

Note: Column 1 - Total Weight Added with Model No. 1 as Reference

Column 2 - Change in Weight within Each Basic Geometrical Shape (ie. Models 3, 6, 9, 12, and 15)

Column 3 - Change in Weight Through the Changing Geometrical Shapes (Model 3 as Reference)

TABLE VII

WEIGHTS OF MATERIAL ADDED OVER THE INTACT CASE

Model Number	Weight Change in way of Hole (grains)
2	- 330.2
3	- 99.6
4	- 91.6
5	- 83.6
6	- 54.3
7	- 26.3
8	- 0.3
9	- 9.0
10	+ 39.0
11	+ 83.0
12	+ 36.3
13	+ 104.3
14	+ 166.3
15	+ 81.6
16	+ 169.6
17	+ 249.6

Note: 1. Intact case is defined as a model with no hole and with two ring frame strips on each side over the location where the hole would be cut.

2. Plus sign indicates material in excess of intact case.

2. Fringe Order Data

The following tables are the results of examining the magnified negatives.

TABLE VIII

SUMMARY OF DATA FOR MODELS 1 AND 2

Model Number	Position	Fringe Order	Model Number	Position	Fringe Order
1a	000	6 T	1b	000	9 1/2 C
	090	16 3/4 C		090	3 1/2 T
	180	6 T		180	9 1/2 C
	270	16 3/4 C		270	3 1/2 T
2a	000	3 1/4 T	2b	000	6 1/2 C
	090	9 1/2 C		090	1 3/4 T
	180	3 1/4 T		180	6 1/2 C
	270	9 1/2 C		270	1 3/4 T

Note: Model number one loadings were 1000 lbs for the "1a" position and 500 lbs for the "1b" position. All other models were loaded at 700 lbs and 350 lbs for the "a" position (parallel to the frames) and "b" position (perpendicular to the frames) respectively.

C - Compression

T - Tension

TABLE IX

SUMMARY OF DATA FOR CIRCULAR REINFORCED MODELS

Model Number	Position	Fringe Order	Model Number	Position	Fringe Order
3a	000	5 1/4 T	3b	000	7 1/2 C
	090	12 1/4 C		090	2 1/4 T
	180	5 1/4 T		180	7 1/2 C
	270	12 1/4 C		270	2 1/4 T
6a	000	5 3/4 T	6b	000	9 C
	090	13 C		090	2 3/4 T
	180	5 3/4 T		180	9 C
	270	14 C		270	3 1/4 T
9a	000	6 1/4 T	9b	000	11 C
	090	15 C		090	3 1/4 T
	180	6 1/4 T		180	11 C
	270	15 C		270	3 1/4 T
12a	000	5 3/4 T	12b	000	11 1/2 C
	090	16 C		090	3 1/4 T
	180	5 1/2 T		180	11 1/2 C
	270	16 C		270	3 1/4 T
15a	000	6 T	15b	000	12 C
	090	14 C		090	3 1/2 T
	180	6 T		180	11 C
	270	15 C		270	3 1/2 T

C - Compression, T - Tension

TABLE X

SUMMARY OF DATA FOR SMALL ELLIPTICAL REINFORCED MODELS

Model Number	Position	Fringe Order	Model Number	Position	Fringe Order
4a	000	5 1/2 T	4b	000	7 1/2 C
	090	12 1/2 C		090	2 1/2 T
	180	5 1/4 T		180	7 1/4 C
	270	12 1/2 C		270	2 3/4 T
7a	000	5 1/4 T	7b	000	7 1/2 C
	090	12 C		090	3 T
	180	5 3/4 T		180	8 1/2 C
	270	13 C		270	3 1/4 T
10a	000	4 3/4 T	10b	000	7 1/2 C
	090	12 1/2 C		090	2 3/4 T
	180	4 3/4 T		180	8 C
	270	13 1/2 C		270	3 T
13a	000	4 3/4 T	13b	000	8 C
	090	13 C		090	3 1/2 T
	180	4 3/4 T		180	8 C
	270	14 C		270	3 1/4 T
16a	000	4 1/2 T	16b	000	8 1/4 C
	090	12 1/2 C		090	3 1/2 T
	180	5 1/4 T		180	8 C
	270	13 1/2 C		270	3 1/4 T

C - Compression, T - Tension

TABLE XI

SUMMARY OF DATA FOR LARGE FILLET RADIUS REINFORCED MODELS

Model Number	Position	Fringe Order	Model Number	Position	Fringe Order
5a	000	5 1/2 T	5b	000	7 1/2 C
	090	12 1/2 C		090	2 1/2 T
	180	5 1/2 T		180	7 C
	270	12 1/2 C		270	2 1/2 T
8a	000	6 T	8b	000	7 1/2 C
	090	13 1/4 C		090	3 T
	180	5 T		180	8 1/2 C
	270	13 1/2 C		270	3 T
11a	000	4 3/4 T	11b	000	8 1/4 C
	090	13 1/2 C		090	3 T
	180	4 3/4 T		180	8 1/4 C
	270	13 C		270	3 T
14a	000	4 1/2 T	14b	000	8 C
	090	14 C		090	2 3/4 T
	180	4 3/4 T		180	8 C
	270	13 C		270	3 T
17a	000	4 1/4 T	17b	000	8 1/4 C
	090	14 C		090	3 1/4 T
	180	5 1/2 T		180	8 1/4 C
	270	14 C		270	3 1/4 T

C - Compression, T - Tension

TABLE XII

SUPERPOSITION OF LOADINGS FOR MODELS 1 AND 2

Model Number	Average Fringe Order On Vertical Axis	Horizontal Axis	Stress Concentration Factor
1	3 1/2 C	13 C	3.72
2	3 1/4 C	7 3/4 C	2.38

C - Compression

T - Tension

TABLE XIII

SUPERPOSITION OF LOADINGS FOR CIRCULAR REINFORCED MODELS

Model Number	Average Fringe Order On Vertical Axis	Horizontal Axis	Stress Concentration Factor
3	2 1/4 C	10 C	4.45
6	3 1/4 C	10 1/2 C	3.23
9	4 3/4 C	11 3/4 C	2.48
12	5 7/8 C	12 3/4 C	2.17
15	5 1/2 C	11 C	2.00

TABLE XIV

SUPERPOSITION OF LOADINGS FOR SMALL ELLIPTICAL REINFORCED MODELS

Model Number	Average Fringe Order On Vertical Axis	Horizontal Axis	Stress Concentration Factor
4	2 C	9 7/8 C	4.94
7	2 1/2 C	9 3/8 C	3.75
10	3 C	10 1/8 C	3.38
13	3 1/4 C	10 1/8 C	3.12
16	3 1/8 C	9 5/8 C	2.96

TABLE XV

SUPERPOSITION OF LOADINGS FOR LARGE ELLIPTICAL REINFORCED MODELS

Model Number	Average Fringe Order On Vertical Axis	Horizontal Axis	Stress Concentration Factor
5	1 3/4 C	10 C	5.71
8	2 1/2 C	10 3/8 C	4.15
11	3 C	10 3/4 C	3.58
14	3 3/8 C	10 5/8 C	3.15
17	3 3/8 C	10 3/4 C	3.19

MODEL THICKNESSES

The following average model thicknesses have been determined by use of a micrometer in the region surrounding the circular hole as the reinforcements were added. These values are used with equation (20) to determine the stress.

TABLE XVI

MODEL THICKNESSES

Model Numbers	Number of Glue Lines	Total Average Thickness (h)
1,2	0	0.245 inches
3,4,5	2	0.408 inches
6,7,8	3	0.490 inches
9,10,11	4	0.575 inches
12,13,14	5	0.655 inches
15,16,17	6	0.735 inches

TABLE XVII

SUMMARY OF STRESS LEVELS FOR CIRCULAR REINFORCED MODELS

Model Number	Superposition of Stresses Vertical Axis	Horizontal Axis	Stress Concentration Factor
3	305 C (psi)	1338 C (psi)	4.45
6	362 C	1170 C	3.23
9	451 C	1115 C	2.48
12	490 C	1064 C	2.17
15	409 C	818 C	2.00

TABLE XVIII

SUMMARY OF STRESS LEVELS FOR SMALL ELLIPTICAL REINFORCED MODELS

Model Number	Superposition of Stresses Vertical Axis	Horizontal Axis	Stress Concentration Factor
4	268 C (psi)	1321 C (psi)	4.94
7	278 C	1045 C	3.75
10	285 C	963 C	3.38
13	271 C	845 C	3.12
16	242 C	715 C	2.96

TABLE XIX

SUMMARY OF STRESS LEVELS FOR LARGE ELLIPTICAL REINFORCED MODELS

Model Number	Superposition of Stresses Vertical Axis	Horizontal Axis	Stress Concentration Factor
5	234 C (psi)	1338 C (psi)	5.71
8	278 C	1158 C	4.15
11	285 C	1021 C	3.58
14	282 C	885 C	3.15
17	251 C	800 C	3.19

TABLE XX

SUMMARY OF STRESS LEVELS FOR ALL MODELS

Model Number	Superposition of Stresses Vertical Axis	Horizontal Axis	Stress Concentration Factor
1	780 C (psi)	2898 C (psi)	3.72
2	725 C	1725 C	2.38
3	305 C	1338 C	4.45
4	268 C	1321 C	4.94
5	234 C	1338 C	5.71
6	362 C	1170 C	3.23
7	278 C	1045 C	3.75
8	278 C	1158 C	4.15
9	451 C	1115 C	2.48
10	285 C	963 C	3.38
11	285 C	1021 C	3.58
12	490 C	1064 C	2.17
13	271 C	845 C	3.12
14	282 C	885 C	3.15
15	409 C	818 C	2.00
16	242 C	715 C	2.96
17	251 C	800 C	3.19

Equation (20) was used to determine these values.

$$\sigma_t = \pm \frac{fn}{h} \qquad (20)$$

where:

σ_t - Tangential Stress on the Free Boundary

f - Fringe Constant (54.6 lbs/in/order)

h - Thickness of model from Table XVI

n - Order of Interference from Tables XII to XV.

3. Comparison of Photoelastic and Strain Gage Techniques

Upon completion of the use of the models, a cut was taken on the small elliptically reinforced model hole so as to true up the edges. A strain gage was then mounted on one side of the horizontal axis and the model loaded to 700 pounds in line with the frames.

The photograph in Figure XXIII shows the fringe pattern with the strain gage mounted and the model under compression.

The strain gage had the following characteristics:

Gage Type: EA - 13 - 250BB - 120

Resistance: 120 ± 0.2 ohms

Gage Factor: 2.095 ± 0.5%

Lot Number: A14AF46

In a quarter bridge circuit using an identical gage as the external dummy, the strain was 2670 $\mu\epsilon$ when the fringe order was 16 on the free boundary.

By equation (20): $\sigma_t = \frac{nf}{h} = \frac{(16)(54.6)}{0.735} = 1190$ psi

From the Strain Gage: $\sigma_t = \epsilon E = 2670 \times 10^{-6} \times 450{,}000$

$= 1202$ psi

This shows an agreement of about 1% in the two techniques of experimental stress analysis. This result is much closer than anticipated.

D. ORIGINAL DATA

Fringe Pattern Photographs

The fringe orders have been estimated to the nearest one quarter order on the four cardinal axes. To aid in the accuracy the negative for each model from the Polaroid Type 55 P/N (Positive/Negative) Film was projected such that it was enlarged at least ten times. This magnification effect was necessary in order to determine the small changes caused by each additional thickness of reinforcement material. The pictures became progressively more difficult to analyze as successive layers of reinforcement were cemented to each of the three basic geometrical foundation pieces.

A reference fringe order was determined for each model as it was being loaded and so noted for evaluation of the negatives.

FIGURE XVII

FRINGE PATTERNS FOR CALIBRATION DISKS AND MODEL 1 AND 2

SMALL CALIBRATION DISK

LARGE CALIBRATION DISK

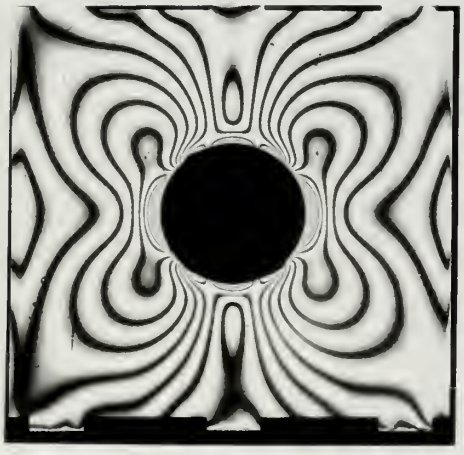

MODEL 1a

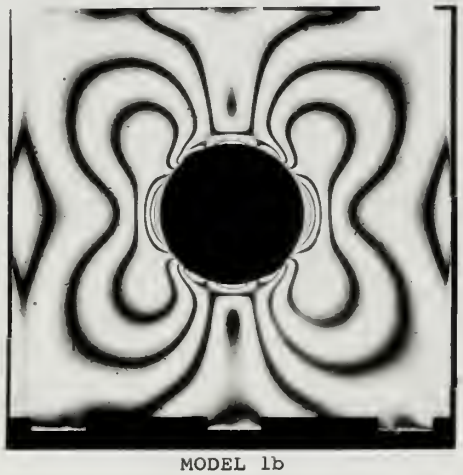

MODEL 1b

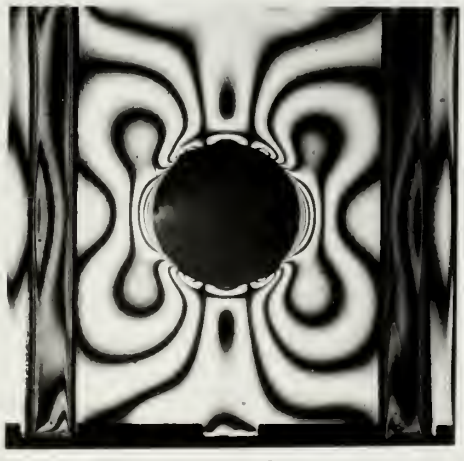

MODEL 2a

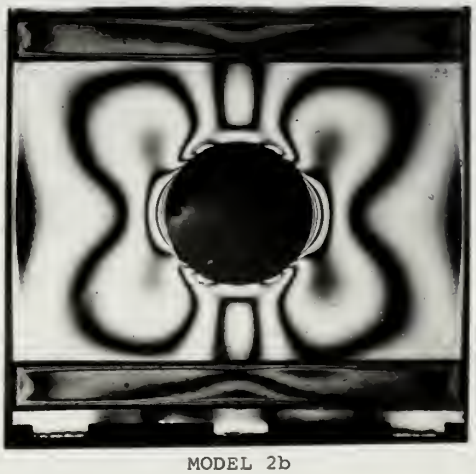

MODEL 2b

FIGURE XVIII

FRINGE PATTERNS FOR TWO REINFORCEMENT THICKNESSES

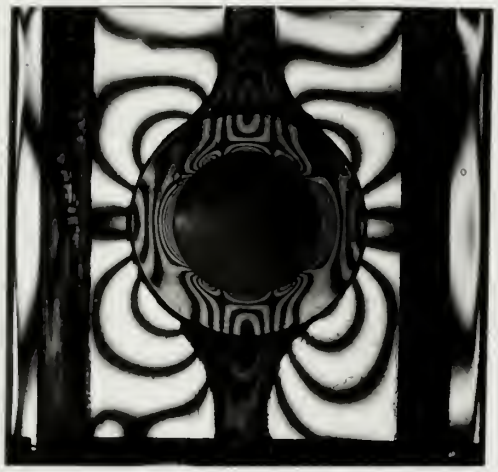

MODEL 3a

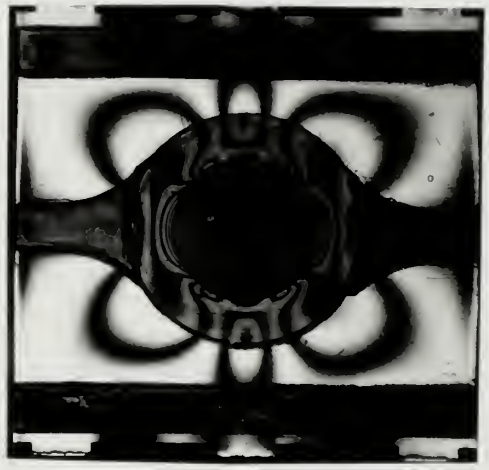

MODEL 3b

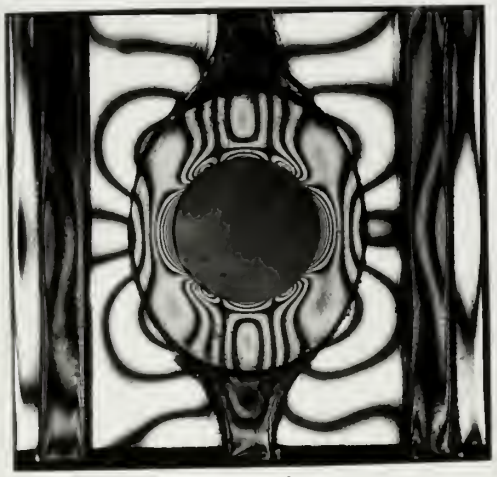

MODEL 4a

MODEL 4b

MODEL 5a

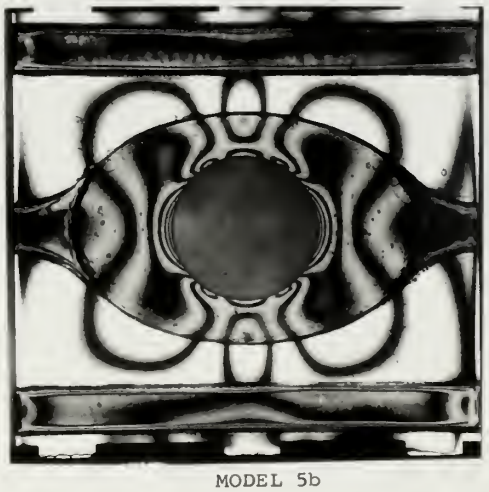

MODEL 5b

FIGURE XIX

FRINGE PATTERNS FOR THREE REINFORCEMENT THICKNESSES

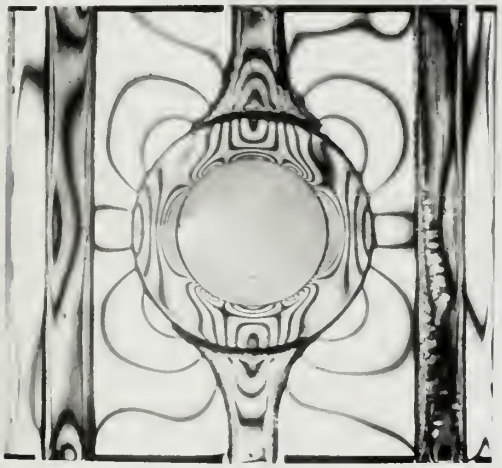

MODEL 6a

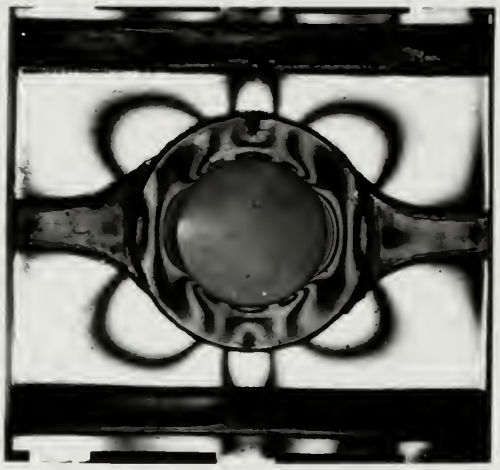

MODEL 6b

MODEL 7a

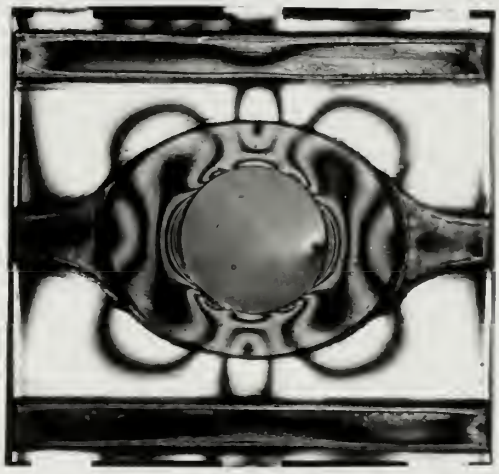

MODEL 7b

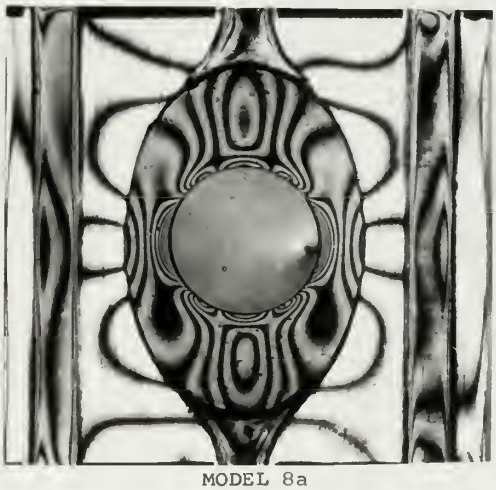

MODEL 8a

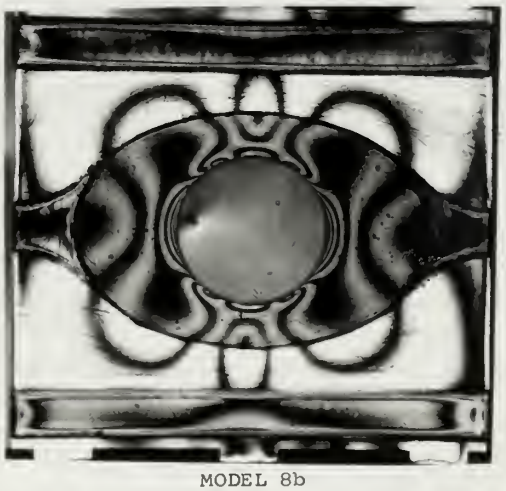

MODEL 8b

FIGURE XX

FRINGE PATTERNS FOR FOUR REINFORCEMENT THICKNESSES

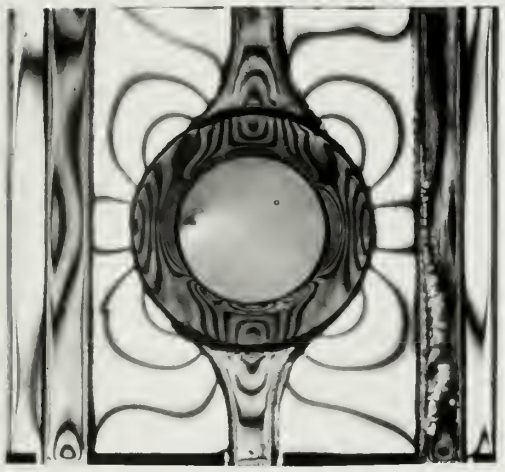

MODEL 9a

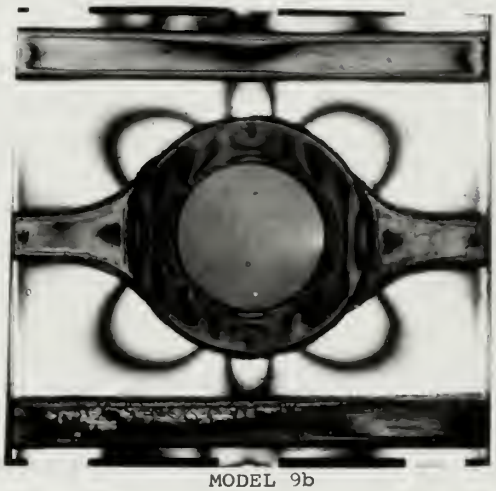

MODEL 9b

MODEL 10a

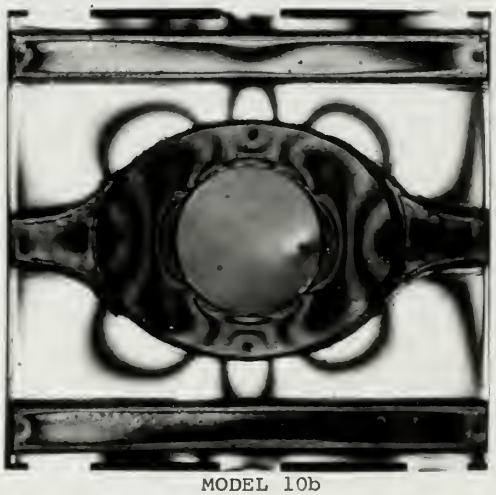

MODEL 10b

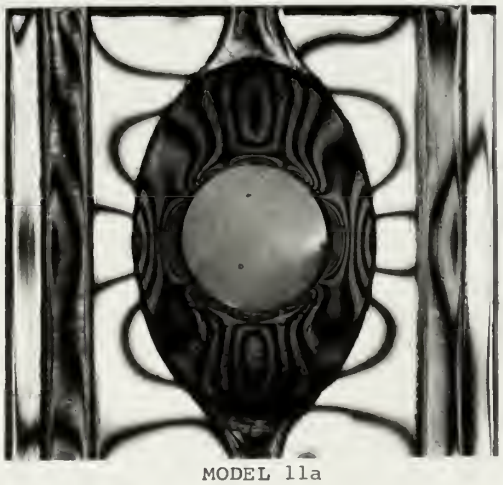

MODEL 11a

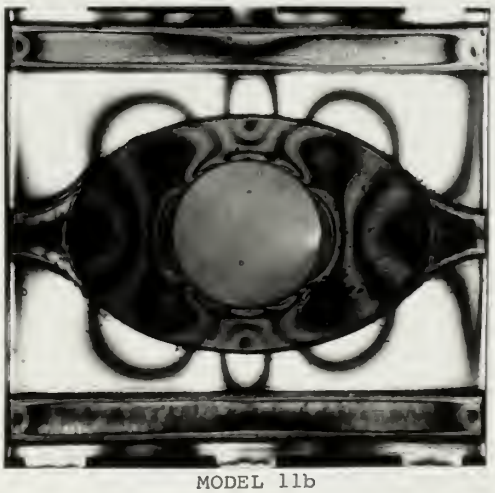

MODEL 11b

FIGURE XXI

FRINGE PATTERNS FOR FIVE REINFORCEMENT THICKNESSES

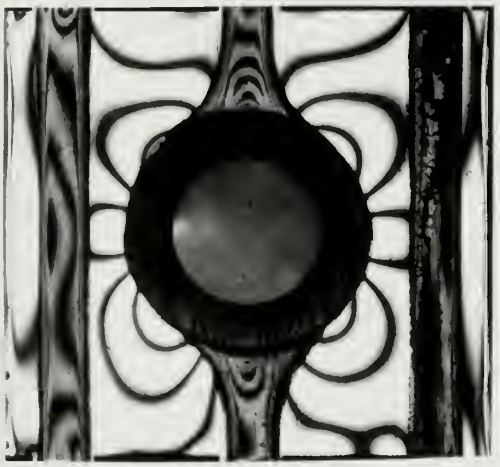

MODEL 12a

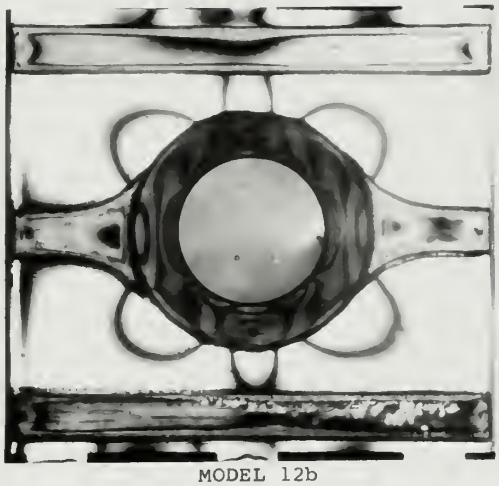

MODEL 12b

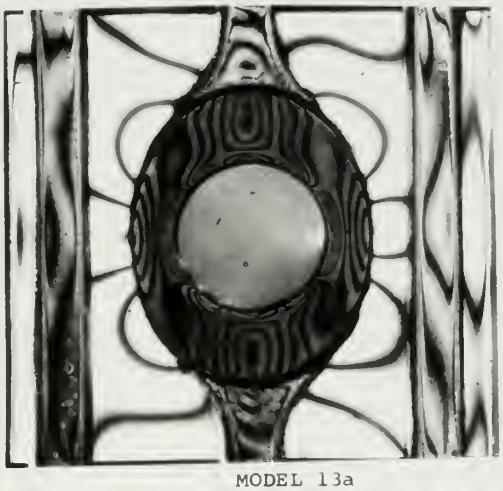

MODEL 13a

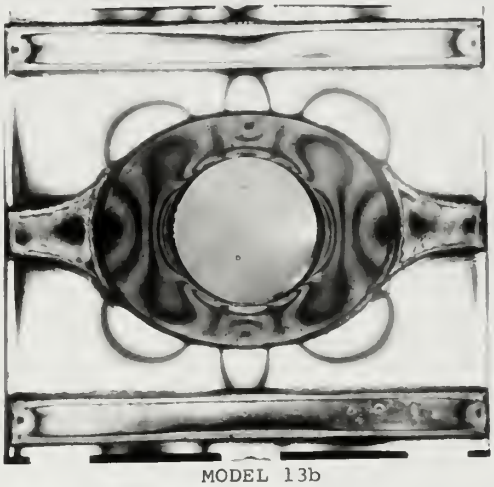

MODEL 13b

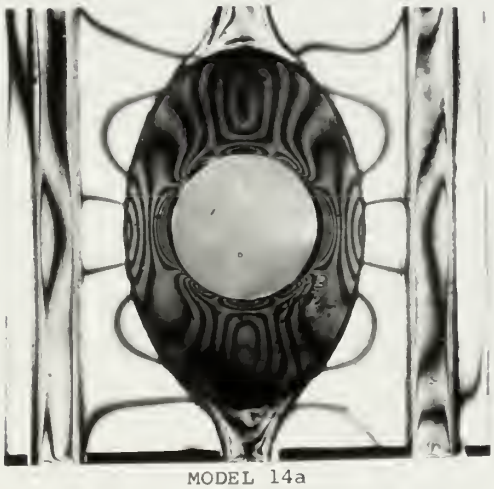

MODEL 14a

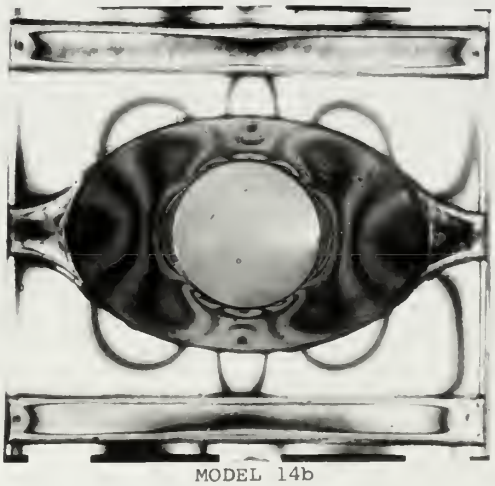

MODEL 14b

FIGURE XXII

FRINGE PATTERNS FOR SIX REINFORCEMENT THICKNESSES

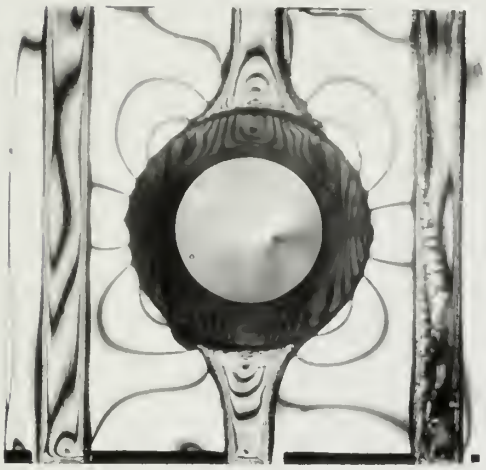

MODEL 15a

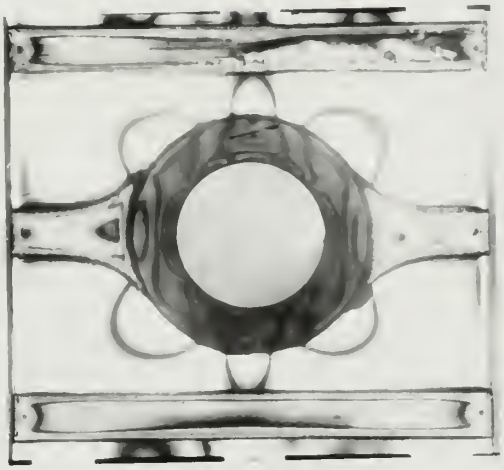

MODEL 15b

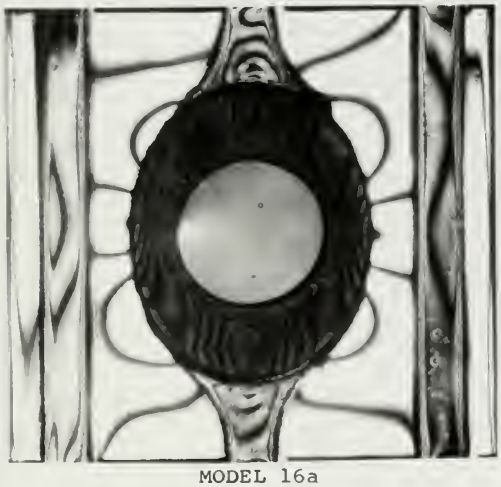

MODEL 16a

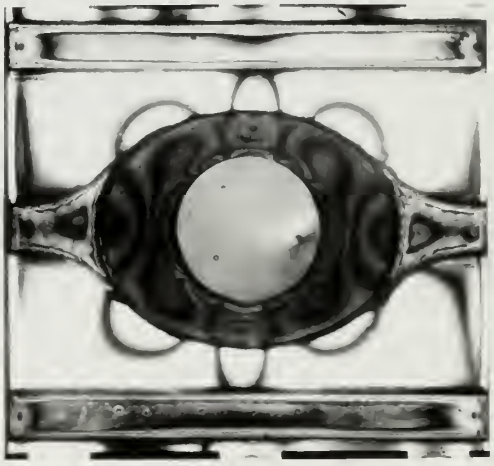

MODEL 16b

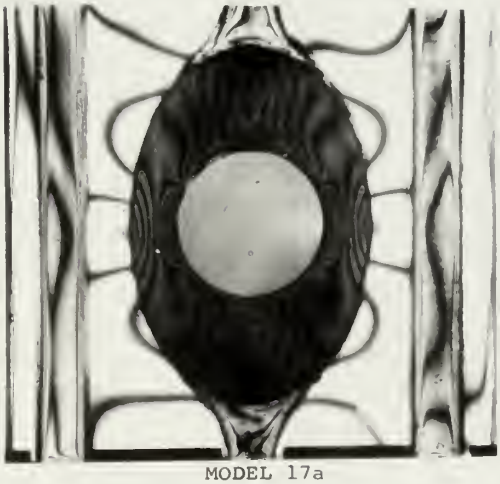

MODEL 17a

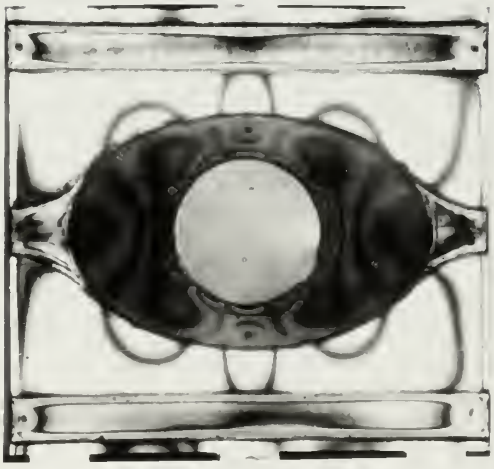

MODEL 17b

FIGURE XXIII

FRINGE PATTERN AND STRAIN GAGE

E. REFERENCES

1. Coker, E.G., and Filon, L.N.G., TREATISE ON PHOTOELASTICITY, Cambridge University Press, 1931.
2. Dally, J.W., and Riley, W.F., EXPERIMENTAL STRESS ANALYSIS, McGraw - Hill, New York, N.Y., 1965. Pages 217-220.
3. Durelli, A.J., "DISTRIBUTION OF STRESSES IN PARTIAL COMPRESSION", Proceedings of the Thirteenth Semi-Annual Eastern Photoelasticity Conference, June, 1941. Pages 25-37.
4. Durelli, A.J., and Riley, W.F., INTRODUCTION TO PHOTOMECHANICS, Prentice - Hall, Englewood Cliffs, N. J., 1965. Pages 63-68.
5. Frocht, M.M., PHOTOELASTICITY, Volume I, John Wiley & Sons, Inc., New York, N. Y., 1941. Pages 134-155.
6. Frocht, M.M., PHOTOELASTICITY, Volume II, John Wiley & Sons, Inc., New York, N. Y., 1948. Pages 140-146.
7. Hetenyi, M., HANDBOOK OF EXPERIMENTAL STRESS ANALYSIS, John Wiley & Sons, Inc., New York, N. Y., 1950. Pages 839-840 and 863-874.
8. Jessop, H.T., and Harris, F.C., PHOTOELASTICITY PRINCIPLES & METHODS, Dover Publications, Inc., New York, N. Y., 1949. Pages 63-65, 68.
9. Murray, W.M., "Class Notes on Experimental Stress Analysis", Subject 2.652, Massachusetts Institute of Technology, 1966.

10. Murray, W.M., and Stein, P., STRAIN GAGE TECHNIQUES, Lecture and Laboratory Exercises, Massachusetts Institute of Technology, 1961.

11. Solakian, A., "PHOTOELASTIC MODELS WITH CEMENTED ELEMENTS", PHOTOELASTIC JOURNAL, Volume VI, No. 1, 1938.

12. Timoshenko, S., and Goodier, J.N., THEORY OF ELASTICITY, McGraw - Hill, New York, N. Y., 1951. Pages 107-109.